

Detecting outlying demand in multi-leg bookings for transportation networks

Nicola RENNIE^{a,*}, Catherine CLEOPHAS^b, Adam M. SYKULSKI^c, and Florian DOST^{d,e}

^aSTOR-i Centre for Doctoral Training, Lancaster University, LA1 4YW, UK.
(n.rennie@lancaster.ac.uk)

^bInstitute for Business, Christian-Albrechts-University Kiel, Kiel, Germany.
(cleophas@bwl.uni-kiel.de)

^cDept. of Mathematics and Statistics, Lancaster University, LA1 4YF, UK.
(a.sykulski@lancaster.ac.uk)

^dInstitute of Business and Economics, Brandenburg University of Technology, 03046 Cottbus, Germany. (florian.dost@b-tu.de)

*Corresponding Author: Nicola Rennie (n.rennie@lancaster.ac.uk)

Abstract

Network effects complicate demand forecasting in general, and outlier detection in particular. For example, in transportation networks, sudden increases in demand for a specific destination will not only affect the legs arriving at that destination, but also connected legs nearby in the network. Network effects are particularly relevant when transport service providers, such as railway or coach companies, offer many multi-leg itineraries. In this paper, we present a novel method for generating automated outlier alerts, to support analysts in adjusting demand forecasts accordingly for reliable planning. To create such alerts, we propose a two-step method for detecting outlying demand from transportation network bookings. The first step clusters network legs to appropriately partition and pool booking patterns. The second step identifies outliers within each cluster to create a ranked alert list of affected legs. We show that this method outperforms analyses that independently consider each leg in a network, especially in highly-connected networks where most passengers book multi-leg itineraries. We illustrate the applicability on empirical data obtained from Deutsche Bahn and with a detailed simulation study. The latter demonstrates the robustness of the approach and quantifies the potential revenue benefits of adjusting for outlying demand in networks.

Keywords: Analytics; Forecasting; Outlier detection; Clustering; Simulation.

1 Introduction and State of the Art

Transport service providers such as railways (Yuan et al., 2018) or long-distance coach services (Augustin et al., 2014) offer a large number of interconnected legs that let passengers travel along a multitude of itineraries. For example, the Deutsche Bahn long-distance network consists of over 1,000 train stations, letting the provider offer more than 110,000 origin-destination combinations. The numbers grow further when accounting for alternative transfer itineraries and for multiple departures per day. Figure 1 shows the empirical distribution of the number of legs included in itineraries that passengers booked with Deutsche Bahn in November 2019. Only 7% of passengers booked single-leg itineraries, whereas almost half of all booked itineraries span five or more legs.

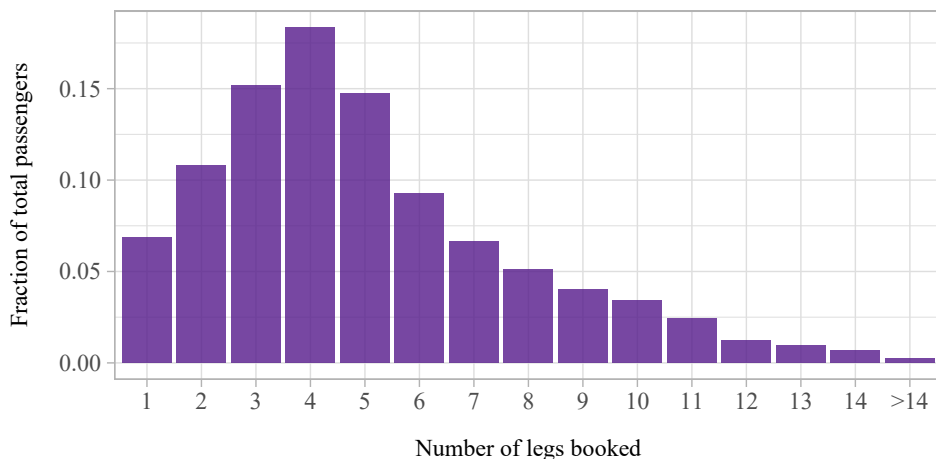


Figure 1: Distribution of number of legs per booked itinerary

When customers predominantly book multi-leg itineraries, offer optimisation becomes more difficult. In the wider revenue management (RM) literature, Klein et al. (2020) reviews how single-leg practices generalise to the network setting for capacity-based RM. Weatherford (2016) surveys RM forecasting methods and particularly considers itinerary-level forecasting for airlines. Further contributions, e.g. Weatherford and Belobaba (2002) and Rennie et al. (2021), demonstrate the negative effects of inaccurate demand forecasts on revenue performance, but neglect network effects. Little existing research however can be found on accounting for demand outliers in revenue management. For historical hotel booking data, Weatherford and Kimes (2003) discuss a simple method of removing observations that are more than $\pm 3\sigma$ away from the mean. Rennie et al. (2021) apply functional analysis to detect outliers on the single-leg level. Outside the RM domain, Barrow

and Kourentzes (2018) also propose a functional approach for outlier detection in call arrival forecasting, but none of these aforementioned works explicitly consider outliers in the multi-leg or network setting.

Outside of RM, outlier detection in networks often focuses on identifying outlying parts of the network. Fawzy et al. (2013) use this approach in wireless sensor networks to find faulty nodes. Ranshous et al. (2015) provide an overview of the extension to identifying outlying nodes in the case where the network changes over time. Most of these works on dynamic networks look at a single time series connected to each node, rather than a set of time series (e.g. booking patterns for multiple departures) as would be observed in a transportation network.

Network bookings challenge outlier detection in two ways: On the one hand, demand outliers on the itinerary level affect multiple legs included in the itinerary. On the other hand, such outliers may not be recognisable given noise from other itineraries when considering the leg’s bookings in isolation. The impact of outliers in the network revenue management setting, and how to identify them, is an open problem. This paper focuses on identifying short-term systematic changes in demand in multi-leg bookings. We argue that jointly considering highly correlated legs significantly improves the performance of any outlier detection mechanism in networks.

Furthermore, practical network RM often relies on manual forecast adjustments (Currie and Rowley, 2010; Schütze et al., 2020). However, previous research (Lawrence et al., 2006; De Baets and Harvey, 2020) has shown that the resulting judgemental forecasts can be biased and even superfluous. To avoid such collateral damages, we contribute a tool to help determine when outlying demand should be analysed. Perera et al. (2019) note that such forecasting support tools can improve user judgement by reducing complexity for the analyst. Analysts’ time is limited and they are unlikely to have the time to investigate every departure which is flagged as an outlier. In fact, Deutsche Bahn experts estimate that they can reasonably adjust less than 1% of forecasts. This motivates us to aggregate outlier analysis across multiple legs and to focus analysts’ attention by constructing a ranked alert list. We consider an outlier as more critical if it indicates a larger demand shift and if it is identified across multiple legs.

Here, the term *departure* indicates a journey that leaves the origin station at a unique time and date. We term a unit sold as a *booking*, and the accumulation of bookings across the booking horizon as a *booking pattern*. Booking patterns may be reported per resource (e.g. per leg), or per product (e.g. per itinerary). We suggest to aggregate and analyse booking patterns from multiple *legs* as opposed to *itineraries* based on two considerations. First, when there are many possible

itineraries in a large network, each individual itinerary only receives a small number of bookings on average, challenging any data analysis. Secondly, when offering a large number of potential itineraries, providers rarely store all booking patterns on an itinerary level. When applying capacity-based RM, booking patterns are stored on the leg level to ensure the availability of capacity on each leg of a requested itinerary.

In the examples given in this paper, we focus on analysing booking patterns from railway networks. Nevertheless, the proposed approach is applicable to any area of transport planning where customers can book products based on connecting multiple resources.

In summary, this paper contributes (i) a method for identifying network legs that will benefit from joint outlier detection; (ii) a method to aggregate outlier detection across any number of legs to create a ranked alert list; (iii) a demonstration of applicability on empirical railway booking data; (iv) a wide-ranging simulation study that evaluates the method’s performance on various demand scenarios; (v) a study that quantifies the potential revenue improvement from adjusting the forecast to detected outlier demand.

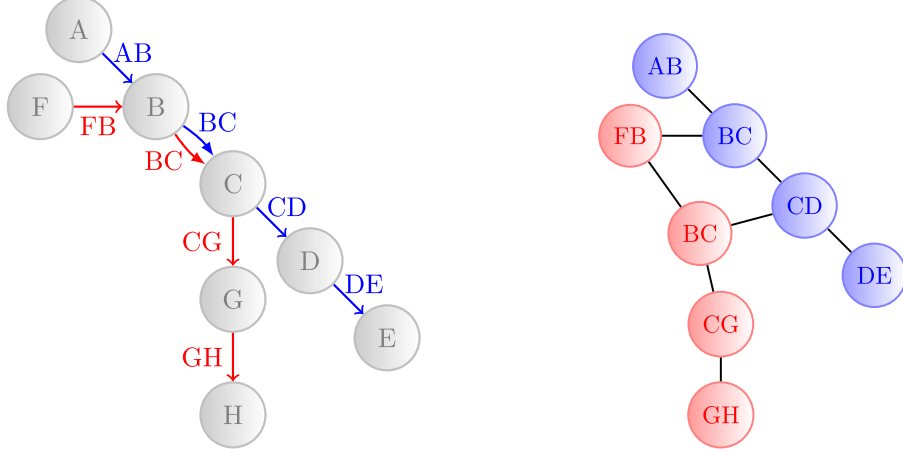
2 Method

In transportation networks, certain legs share common outliers, as a common set of passengers traverses them. This raises the question of which legs to consider jointly for outlier detection. Neither considering each leg independently, nor jointly considering the network as a whole will create the best results when a network spans multiple regions that differ strongly in expected demand. Therefore, we propose to first *cluster* legs such that (i) legs in the same cluster share common outliers and can be considered jointly for outlier detection, and (ii) legs in different clusters experience independent demand outliers and can be considered separately. Subsequently, we suggest a method for aggregating booking information within a cluster of similar legs, and then ranking identified outliers by *severity* rather than simply providing a binary classification.

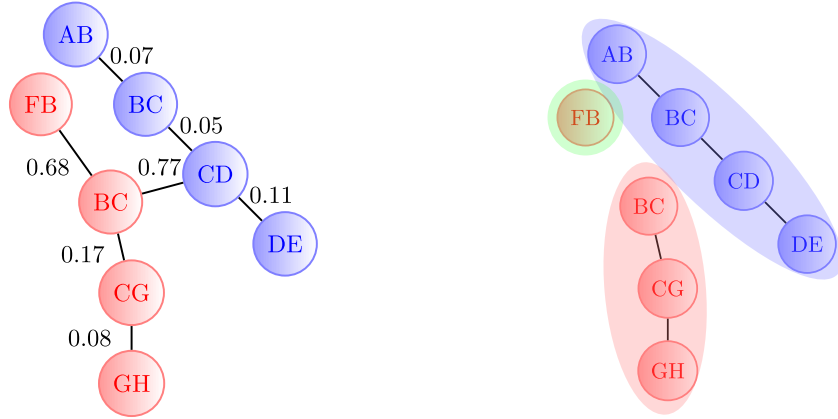
2.1 Correlation-based minimum spanning tree clustering

To cluster legs based on the correlations in observed bookings, we first represent the network as a graph where nodes represent the stations and edges represent the legs of a journey. We shall illustrate our correlation-based clustering approach on the simple network shown in Figure 2a. In this example, two train lines (red and blue)

intersect at two stations (B and C). The red train arrives at stations B and C before the blue train, which creates two possible transfer connections for passengers: (i) switch from red to blue at B, (ii) switch from red to blue at C. Transfers from the blue to red train are not feasible.



(a) Original graph where nodes represent stations (b) Inverted graph where nodes represent legs



(c) Minimum spanning tree with edge weights (d) Clusters obtained in inverted graph

Figure 2: Correlation-based minimum spanning tree clustering

Common graph clustering algorithms seek to cluster the nodes of the graph (Schaeffer, 2007). In contrast, we wish to cluster similar legs, which correspond to edges in the original graph 2a. Hence, we invert the graph to make existing clustering algorithms applicable. In this inversion (Figure 2b), the directed edges become nodes e.g. the edge from A to B becomes node AB. The inverted graph

features an undirected edge between two nodes (two legs of the original graph) when:

- both legs are in the same train line and share a common station, e.g., legs CD and DE are connected through station D.
- the legs are in different train lines but share a common transfer station where a connection is possible, e.g., leg FB (red line) and BC (blue line) are connected through station B. However, AB (blue line) and BC (red line) would not be connected by an edge as no connection can be made between them (as we have assumed the red train arrives at B and C before the blue train).

In theory, this transformation could also include an edge between legs that share a common entry or exit node e.g. FB (red line) and AB (blue line), or CG (red line) and CD (blue line). However, in clustering both empirical and simulation data, we found that correlations between these types of legs were not sufficiently high to impact the outcome. Further, such pairs of legs would never occur in the same itinerary, such that no itinerary forecast adjustment would apply to both legs.

The algorithm aims to assign legs that experience *similar bookings* to the same cluster and legs that experience *dissimilar bookings* to separate clusters. A corresponding metric only needs to consider similarity between adjacent legs, which share a connecting station, since edges do not exist in the inverted graph otherwise. We define the **common traffic ratio** between two adjacent legs as the proportion of total demand that relates to itineraries over both legs. That is, for two legs ij and jk , we define the common traffic ratio, $r(ij, jk)$, to be:

$$r(ij, jk) = \frac{D_{ik}}{D_{ij} + D_{jk} + D_{ik}}, \quad (1)$$

where D_{ij} is the demand for itinerary ij , and D_{ik} is the total demand for all itineraries which include both legs ij and jk . If all passengers book itineraries that traverse both legs, then $r(ij, jk) = 1$. Conversely, if no passengers book journeys that traverse both legs, then $r(ij, jk) = 0$.

When the number of passengers booking each itinerary is known, we can directly compute $r(ij, jk)$. However, in practice, this information is rarely available. For example, booking patterns may not be stored on the itinerary level, or feature too small numbers when the number of itineraries far exceeds the number of legs. In such cases, we propose to estimate similarity from the correlation between bookings on legs. To that end, we compute the functional dynamical correlation (Dubin and Müller, 2005) – see Appendix A.1. Unlike more common statistical correlation measures, such as Pearson correlation, functional dynamical correlation does not

assume a specific type of relationship between variables (e.g. linearity). It also accounts for the time dependency between observations in the booking horizon, including the differing length of intervals between observations. For example, in the empirical data described in Section 3, the time between booking intervals decreases as the departure date approaches. Further, alternative measures for calculating correlations from functional data (such as functional canonical correlation) often make restrictive assumptions, which real data does not fulfil (He et al., 2003). In Appendix D.1, we benchmark the clustering algorithm under different correlation measures.

To represent the relationship between legs in the network (the nodes in the inverted graph), we attach edge weights to the inverted graph. The edge weights can be interpreted as distances: The higher the edge weight, the further apart i.e. more dissimilar, the connected nodes are. Hence, we define the edge weights as:

$$w_{(ij,jk)} = 1 - \rho(ij, jk), \quad (2)$$

where $\rho(ij, jk)$ is the correlation between bookings on legs ij and jk . When the share of demand for itineraries is known from itinerary-level data, $\rho(ij, jk)$ can be replaced with $r(ij, jk)$.

We use a minimum spanning tree-based algorithm to allow for clusters of irregular shapes. For example, in Figure 2b, a cluster may include AB and DE because they are in the same line, rather than clustering AB and FB. Minimum spanning tree approaches work well for clusters with irregular boundaries (Zahn, 1971). Alternative approaches (such as k -means), often assume a specific shape of clusters (spherical, for k -means).

A *spanning tree* of a graph is a subgraph that includes all vertices in the original graph and a minimum number of edges, such that the spanning tree is connected. Then, the minimum spanning tree (MST) is the spanning tree with the minimum summed edge weights – see Figure 2c. Since the inverted graph is weighted, we use Prim’s algorithm (Prim, 1957) to calculate the MST – see Appendix A.2 for a detailed introduction.

There are two approaches to obtaining clusters from a minimum spanning tree: (i) pre-defining the number of clusters as k , and removing the $k - 1$ edges with highest weight; or (ii) setting a threshold for the edge weights and remove all edges with weights above some threshold, creating an emergent number of clusters. We implement the threshold-based approach, as this ensures that each cluster has the same minimum level of correlation. In contrast, setting the number of clusters in advance could result in very heterogeneous levels of correlation across clusters. Further, setting k too low may result in legs with dissimilar features being grouped

together. We apply a threshold correlation of 0.5 – the level at which legs are more correlated than they are not. This corresponds to a transformed edge weight of 0.5. In the example given in Figure 2c, this means removing all legs with a weight above 0.5, resulting in the three clusters shown in Figure 2d.

Note that the outlier detection procedure applies to individual clusters, but does not require a particular clustering approach. Hence, alternative approaches, as reviewed in Schaeffer (2007), could be utilised.

2.2 Detecting outliers in clusters of legs

In the remainder of this section, we detail the process of identifying demand outliers within each of the clusters (as defined in Section 2.1) and then quantifying the severity of such outliers. This procedure returns a ranked list of departures, which we term an *alert list*.

To identify which departures should be included in the alert list, we consider the statistical *depth* of their booking patterns. In statistics, depth describes an ordering of observations, where those near the centre of the distribution have higher depth and those far from the centre have lower depth. Functional analysis treats each booking pattern as an observation of a smooth function sampled at discrete time points. The functional depth provides an ordering to this set of smooth functions. The booking pattern with the most central trajectory has the highest depth, and the most outlying trajectories have the lowest depths. By using functional depth, we are not only able to identify outliers caused by changes in *magnitude* of demand, but also in changes to the *shape* of the booking patterns.

The approach presented here can also be implemented with other measures of exceedance, including univariate “threshold” approaches which look at aggregated bookings and ignore the shape of the booking curve. Here, we use *functional depth*, as previous work has found this to be the most effective as an outlier detection mechanism (Rennie et al., 2021).

Consider N departures, observed over L legs. Let $\mathbf{y}_{nl} = (y_{nl}(t_1), \dots, y_{nl}(t_T))$ be the booking pattern for the n^{th} departure on leg l , observed over T booking intervals t_1, \dots, t_T . Let \mathcal{Y}_l be the set of N booking patterns for leg l . For each leg and departure, we calculate the functional depth (Hubert et al., 2012), with respect to the booking patterns for that leg – see Appendix A.3.

For each leg l , we calculate a threshold for the functional depth using the approach of Febrero et al. (2008). This method (i) resamples the booking patterns with probability proportional to their functional depths (such that any outlying patterns are less likely to be resampled), (ii) smooths the resampled patterns, and

(iii) sets the threshold C_l as the median of the 1st percentiles of the functional depths of the resampled patterns. Booking patterns with a functional depth below the threshold C_l are outliers.

We define z_{nl} to be the normalised difference between the functional depth and the threshold:

$$z_{nl} = \frac{C_l - d_{nl}}{C_l}. \quad (3)$$

This transforms the depth measure d_{nl} into a measure of *threshold exceedance*. Values of z_{nl} greater than zero relate to booking patterns classified as outliers. Normalising by the threshold, C_l , ensures the values of z_{nl} are comparable between different legs.

Next we define the sums of threshold exceedances across legs:

$$z_n = \sum_{l=1}^L z_{nl} \mathbb{1}_{\{z_{nl} > 0\}}. \quad (4)$$

We sum only those values of z_{nl} that are greater than zero, to avoid outliers being masked when they occur only in a subset of legs. This sum implicitly accounts for both the size of an outlier – larger outliers further exceeding the threshold, resulting in larger values of z_{nl} – and for the number of legs in which a departure is classified as an outlier (by summing a larger number of non-zero values). To provide an example, Figure 3 shows those values of z_n that exceed zero for a four leg section of the Deutsche Bahn network (to be discussed further in Section 3.2). These values of z_n correspond to departures where the booking pattern for *at least* one leg is identified as an outlier, whereas all other departures have no detected outliers in any leg such that $z_n = 0$.

To create a ranked list of outlier departures, i.e. those with a non-zero sum of threshold exceedances, we assign a severity, θ_n . A higher value of θ_n indicates the departure is more likely to be affected by extreme outlier demand, and hence should be targeted first by RM analysts.

To model the threshold exceedances, we turn to extreme value theory (EVT) – a branch of statistics that deals with modelling rare events i.e. those that occur in the tails of the distribution. There are two common approaches to EVT: (i) block maxima, which examines the maximum value in evenly-spaced blocks of time e.g. annual maxima, and (ii) peaks over threshold, which examines all observations that exceed some threshold (Leadbetter, 1991). The generalised Pareto distribution (GPD) is commonly used to model the tails of distributions in the peaks over threshold approach (Pickands, 1975). Motivated by this, we fit a generalised Pareto distribution (GPD) to the sum of threshold exceedances given in equation (4). The

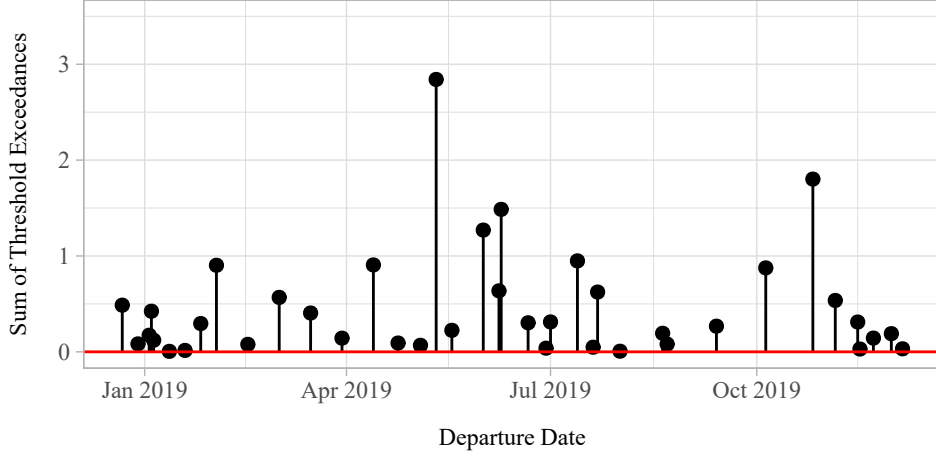


Figure 3: z_n as defined in equation (4) for a four leg section of the Deutsche Bahn network

GPD has three parameters with probability density function:

$$f(x|\mu, \sigma, \xi) \frac{1}{\sigma} \left(1 + \frac{\xi(x - \mu)}{\sigma} \right)^{(-\frac{1}{\xi}-1)}, \quad (5)$$

for

$$x \in \begin{cases} [\mu, \infty) & \xi \geq 0 \\ [\mu, \mu - \frac{\sigma}{\xi}] & \xi < 0. \end{cases} \quad (6)$$

Here, μ specifies the location, σ the scale, and ξ the shape of the distribution. We fit the parameters using maximum likelihood estimation (Grimshaw, 1993), using the R package POT (Ribatet and Dutang, 2019). A kernel density estimate of the empirical distribution of $z_n > 0$ from Figure 3 is shown in Figure 4a. The resulting fitted GPD is shown in Figure 4b. The GPD fit appears to be reasonable compared to the empirical distribution; further analysis in Appendix B.4 supports this.

Two common issues arise in fitting GPDs: (i) the choice of threshold and (ii) the independence of the data points. When the threshold is too low, the assumption of a GPD no longer holds; when it too high, there are too few data points to fit. We select a threshold of 0, i.e., we fit the GPD to values of $z_n > 0$. Rather than change the threshold at GPD level, we control the number of observations the GPD is fitted to by varying the percentile used for the individual leg thresholds, C_l . We choose C_l as suggested by Febrero et al. (2008), and found that this choice worked well and provided sufficient outlying points to fit a GPD both in simulated and empirical data.

To account for the second issue, applications of extreme value theory frequently

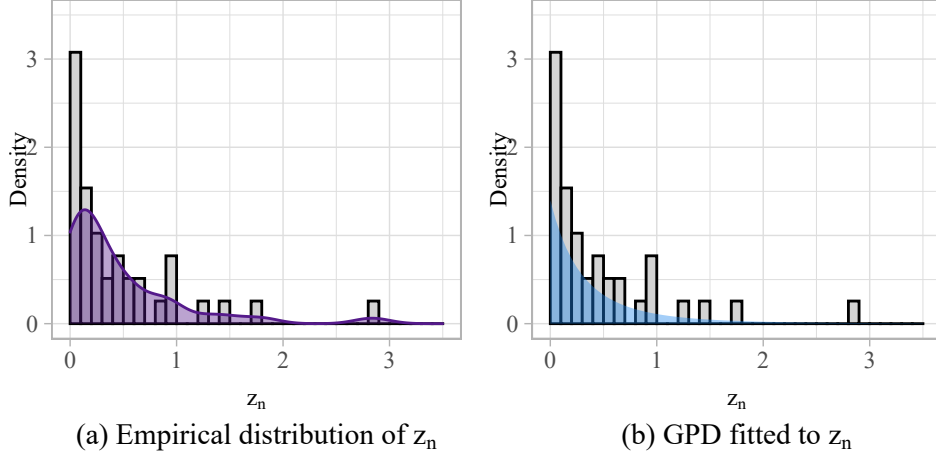


Figure 4: Distribution of z_n values from Figure 3

first *decluster* the peaks over the threshold to ensure independence between observations (Fawcett and Walshaw, 2007). To that end, the analysis may only consider the maximum of two peaks that occur within some small time window. For mobility departures, it is theoretically possible that observed outliers may be dependent; e.g., increased demand caused by Easter not only affects Easter Sunday but also the surrounding days. However, it is also very possible that the outliers are generated by independent events. As we aim to identify outlying departures rather than the underlying events themselves, this argument causes us not to decluster here.

We define θ_n as the non-exceedance probability given by the CDF of the GPD:

$$\theta_n = F_{(\mu, \sigma, \xi)}(z_n) = \begin{cases} 1 - \left(1 + \frac{\xi(z_n - \mu)}{\sigma}\right)^{-\frac{1}{\xi}} & \xi \neq 0 \\ 1 - \exp\left(-\frac{(z_n - \mu)}{\sigma}\right) & \xi = 0 \end{cases} \quad (7)$$

Formally, θ_n is the probability that, given an outlier occurs, the sum of threshold exceedances is at least as large as z_n . Thus, it is *not* the probability that a departure is an outlier. However, we use this non-exceedance probability as a measure of outlier *severity* on a scale of 0 to 1.

Departures with functional depths that do not fall below the threshold on any legs are given a severity of zero i.e. they are classified as regular departures. It is conceivable to estimate the uncertainty of θ_n (Smith, 1985) to determine further levels of criticality e.g. if there are departures with the same outlier severity, the one with smaller uncertainty would be targeted first. However, given the continuous nature of the data, it is unlikely that two departures will have an identical severity. Hence, we leave uncertainty estimates to future research.

From the severity defined in equation (7), we construct a ranked **alert list**

containing all departures with a non-zero outlier severity. Although the functional depth could be directly used to construct the ranked alert list, the severity provides a measure of the difference between each rank and is more easily interpreted by analysts. The top 8 ranked outliers relating to Figure 3, are shown in Table 1.

Ranking	Departure	Severity	Legs with $z_{nl} > 0$
1	11/05/2019	0.985	AB, BC, CD, DE
2	26/10/2019	0.960	AB, BC, CD, DE
3	09/06/2019	0.942	AB, BC, CD, DE
4	01/06/2019	0.922	AB, BC, CD, DE
5	13/07/2019	0.874	AB, BC, CD, DE
6	13/04/2019	0.865	CD, DE
7	02/02/2019	0.864	CD, DE
8	05/10/2019	0.857	AB, BC, CD, DE
\vdots	\vdots	\vdots	\vdots

Table 1: Ranked alert list for cluster = $\{AB, BC, CD, DE\}$

In practice, RM analysts’ time and resources only allow them to examine and adjust controls or forecasts for a limited number of suspicious booking patterns. Further, those departures which (i) exceed the functional depth threshold in only one leg or (ii) exceed the threshold only to a small degree have lower but strictly non-zero severity. These outliers are most likely to be false positives and potentially waste analysts’ time. Hence, we suggest limiting the length of the list used in practice.

There are two approaches to shortening the length of the alert list: (i) only including departures in the alert list if their severity is above some threshold, or (ii) setting a maximum length. Since we wish to control the number of alerts an analyst will receive, we shall analyse outlier detection performance with respect to the maximum length of the alert list. Recall that we classify departures as outliers if and only if their outlier severity exceeds zero. Therefore, if the required length of the alert list exceeds the number of identified outliers, we do not include further departures. Appendix D.2.5 presents further results on the performance of the outlier detection when varying the outlier severity threshold.

3 Empirical study of Deutsche Bahn booking data

To demonstrate the approach described in Section 2, we apply it to empirical data obtained from Deutsche Bahn. We illustrate both the correlation-based clustering approach (in Section 3.1) and the aggregated outlier detection routine (in Section 3.2).

3.1 Clustering legs in the Deutsche Bahn network

We now consider a section of the Deutsche Bahn railway network that consists of two intersecting train lines over a total of 27 stations – see Figure 5. The red train arrives at the connecting stations before the blue train. Hence, the network offers three transfer connections: changing from red to blue at either Fulda, Kassel-Wilhelmshöhe, or Göttingen. This creates 240 potential travel itineraries.

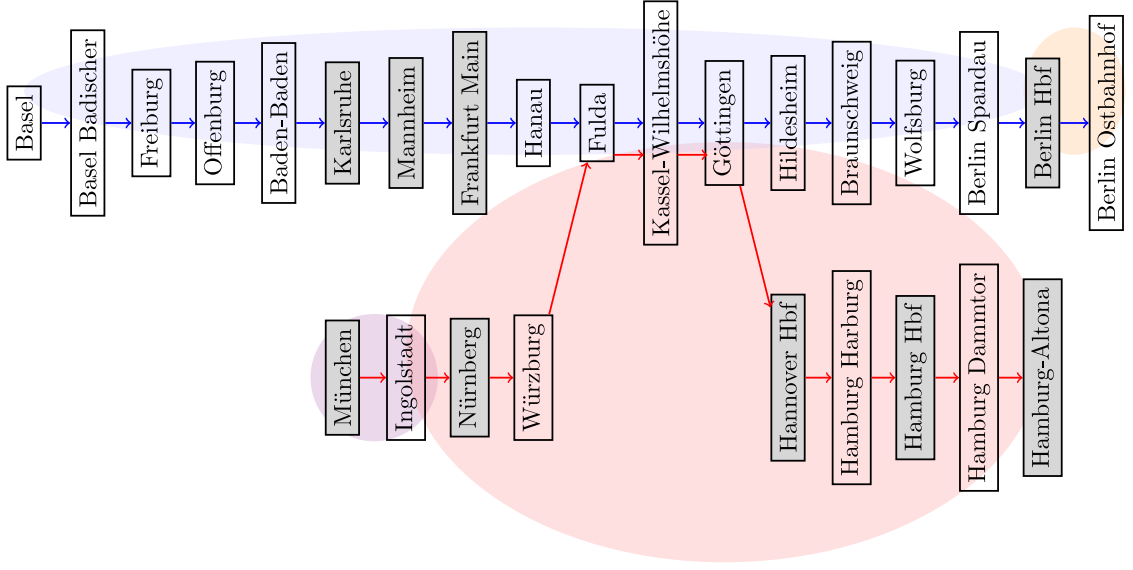
For each leg in this network section, Deutsche Bahn provided 359 booking patterns for departures between December 2018 and December 2019. Each booking pattern ranges over 19 booking intervals; the first observation occurs 91 days before departure.

We firstly apply the correlation-based clustering approach of Section 2.1, using a threshold of 0.5, such that only legs with a minimum correlation of 0.5 can be in the same cluster. In Figure 5a, coloured bubbles indicate the four resulting clusters: Each train line splits into one large and one small cluster.

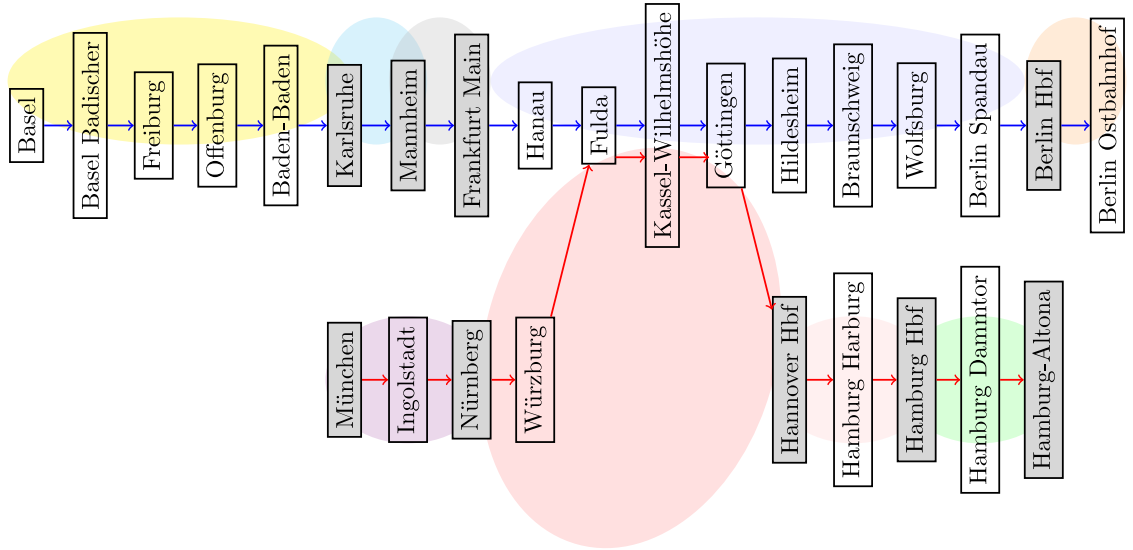
To evaluate clustering on real data, where the true underlying demand for each itinerary is unknown, we use the network topology to check whether resulting clusters are plausible. To that end, we propose the following set of rules:

- Different train lines must be in different clusters. Even when passengers can transfer between lines, we expect relatively few passengers to make the same connection. Further, for forecasting and analyst interventions, it makes sense to consider train lines separately.
- Train lines are further split into different clusters on either side of a major station. As many passengers leave the train at a major station and many *different* passengers board, we shall assume a relatively small proportion of passengers book itineraries that pass a major station. Similarly, given that itinerary demand share is driven by which journeys are most common, and passengers often either board or alight at a major station, it is intuitive to have a cluster that contains the legs between major stations.

Deutsche Bahn assigns an ordinal indicator of importance to each station, ranging from 1 to 7. We define a *major station* to be in *Category 1*. The entire



(a) Correlation-based clustering, $\rho \geq 0.5$



(b) Rule-based cluster

Figure 5: Comparison of correlation-based and rule-based clustering of Deutsche Bahn network

Deutsche Bahn network includes 21 major stations, where the considered network section includes 9. Figure 5b highlights major stations in grey and shows the clusters resulting from the rules listed above.

Whereas the correlation-based clustering returns four clusters, the rule-based clustering returns nine. Nevertheless, the resulting clusters share similar features. Firstly, the two distinct train lines end up in different clusters in either approach. For legs in distinct train lines, correlation tends to be higher between legs that share a transfer station, but not to a convincing extent – correlation is at most 0.22. A correlation threshold of 0.27 creates two clusters (one for each train line). Secondly, the break points for the correlation-based approach are a subset of the break points, i.e., major stations, in the rule-based approach. We conclude that the correlation-based approach achieves similar results as the rule-based approach without expert input - relying only on booking data.

We can formally compare clustering results using the **Normalised Mutual Information (NMI)** (Amelio and Pizzuti, 2015). The NMI is 1 if two clusterings are identical, and 0 if they are completely different (see Appendix A.4 for details). Figure 6a shows the NMI between the correlation- and rule-based approaches while varying the threshold in the correlation-based approach from 0 to 1. This shows that both approaches achieve similar results, with an NMI reaching 0.899. The approaches are generally more similar at higher correlation thresholds (around 0.7), since the rule-based approach generally creates more clusters. Figure 6b compares the number of clusters of the two approaches – as the correlation threshold changes, the number of clusters ranges from 1 (everything in a single cluster) to 28 (each leg in its own cluster), demonstrating the flexibility of the correlation-based approach.

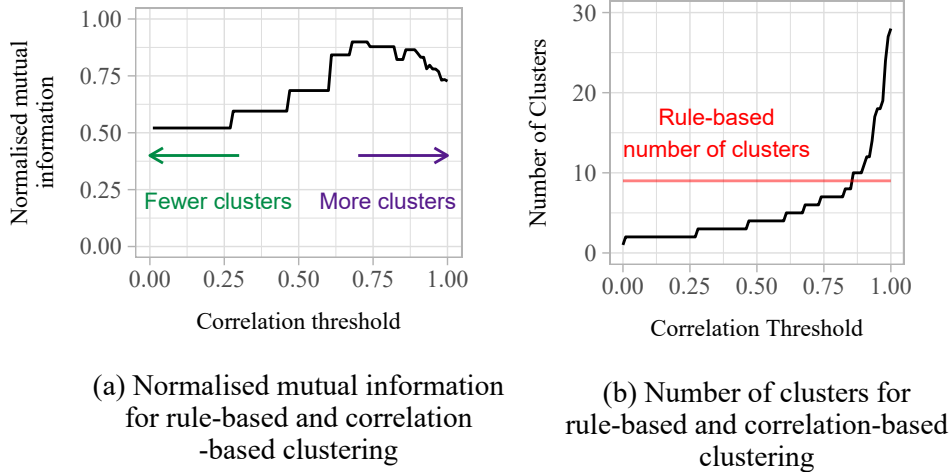


Figure 6: Comparison of rule-based and correlation-based clustering

Here, we applied rule-based clustering only to evaluate the plausibility of the results from correlation-based clustering. We do not advocate for it as a method in itself. A rule-based approach, where the clusters are based on domain experts' cat-

egorisations, would not be able to respond to the evolving importance of stations across different train lines and departure times. Notably, the correlation-based method is not simply a data-driven method for uncovering major stations, but rather for identifying legs where multi-leg itineraries cause similar booking patterns, and thus could change and adapt over time. We further evaluate clustering performance in a simulation study, where the itinerary-level demand is known, in Appendix D.1. The results in the remainder of the paper rely on correlation-based clustering.

3.2 Detecting outliers in multiple legs

We now demonstrate the proposed outlier detection approach on Deutsche Bahn data. Such an analysis cannot precisely judge detection accuracy, given there is no labelled data on genuine outliers. However, this analysis illustrates the full process of outlier detection on empirical data including, e.g., seasonality and underlines practical implications.

We consider a cluster of four legs from the Deutsche Bahn network with stations anonymised and denoted by A, B, C, D, and E. This cluster results from applying the correlation-based clustering to a new section of the Deutsche Bahn network to Figure 5.

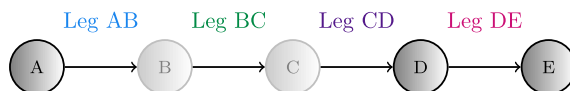


Figure 7: Four leg cluster within the Deutsche Bahn network

Figure 8 shows the booking patterns for each of the four legs; bookings are scaled to be between 0 and 1. From initial visual inspection, the structure of the booking patterns appears similar, with some obvious outliers appearing across multiple legs.

To pre-process the data for outlier detection, we transform the booking patterns by applying a functional regression model (Ramsay and Silverman, 1997). We then apply the outlier detection to the residual booking patterns. In this pre-processing, we correct for three factors: (i) departure day of the week; (ii) departure month of the year; and (iii) the length of the booking horizon.¹

The functional regression fits a mean function to the booking patterns for each

¹Deutsche Bahn offer a regular booking horizon of 6 months, with the first observation of bookings occurring around 3 months before departure. Due to schedule changes, shorter booking horizons of 3 months apply for departures from mid-December to mid-March.

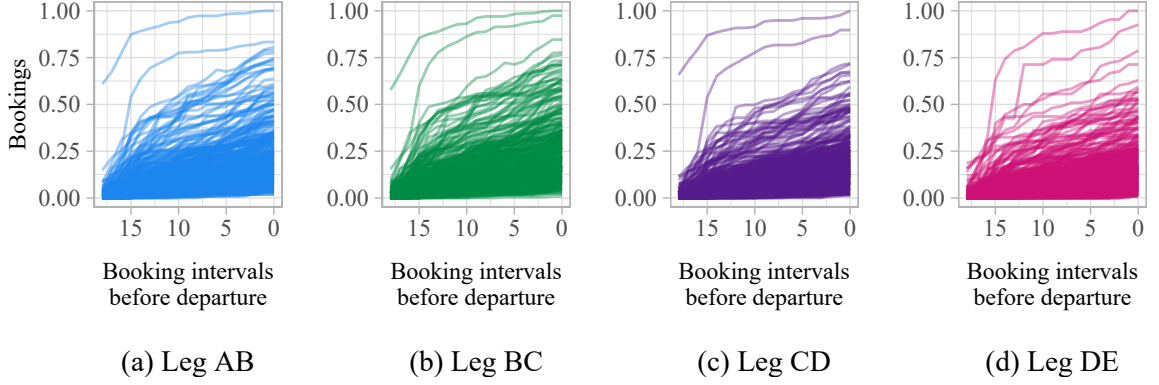


Figure 8: Booking patterns for each leg

different factor in the model. Table 2 in Appendix B.1 compares models including different factors. Let $y_{nl}(t)$ be the n^{th} booking pattern for leg l . Then:

$$\begin{aligned}
 y_{nl}(t) = & \beta_{0l}(t) + \beta_{1l}(t)\mathbb{1}_{Mon_{nl}} + \beta_{2l}(t)\mathbb{1}_{Tue_{nl}} + \beta_{3l}(t)\mathbb{1}_{Wed_{nl}} + \\
 & \underbrace{\beta_{4l}(t)\mathbb{1}_{Thu_{nl}} + \beta_{5l}(t)\mathbb{1}_{Fri_{nl}} + \beta_{6l}(t)\mathbb{1}_{Sat_{nl}}}_{\text{Departure Day of the Week}} + \\
 & \beta_{7l}(t)\mathbb{1}_{Jan_{nl}} + \beta_{8l}(t)\mathbb{1}_{Feb_{nl}} + \beta_{9l}(t)\mathbb{1}_{Mar_{nl}} + \\
 & \beta_{10l}(t)\mathbb{1}_{Apr_{nl}} + \beta_{11l}(t)\mathbb{1}_{May_{nl}} + \beta_{12l}(t)\mathbb{1}_{Jun_{nl}} + \beta_{13l}(t)\mathbb{1}_{Jul_{nl}} + \\
 & \underbrace{\beta_{14l}(t)\mathbb{1}_{Aug_{nl}} + \beta_{15l}(t)\mathbb{1}_{Sep_{nl}} + \beta_{16l}(t)\mathbb{1}_{Oct_{nl}} + \beta_{17l}(t)\mathbb{1}_{Nov_{nl}}}_{\text{Departure Month of the Year}} + \\
 & \underbrace{\beta_{18l}(t)\mathbb{1}_{Shorter Horizon_{nl}}}_{\text{Length of Booking Horizon}} + e_{nl}(t).
 \end{aligned} \tag{8}$$

where e.g., $\mathbb{1}_{Mon_{nl}} = 1$ if departure n relates to a Monday, 0 otherwise. In this model, $\beta_{0l}(t)$ represents the average bookings for Sunday departures in December, with a regular length of booking horizon, and $\beta_{pl}(t)$ for $p > 0$ represent deviations from this mean pattern. The $\beta_{pl}(t)$ are functions of time, which allows for relationships between factors to evolve over the booking horizon. Given that functional depths are calculated independently for each leg, we apply the regression model independently for each leg. The resulting residuals are shown in Appendix B.2, Figure 17.

Functional regression preserves the correlation between different legs, as verified in Appendix C.3, Table 5b. The clustering approach can consider either the correlations between the booking patterns or the residual booking patterns. Given that the functional depths (the basis for the outlier detection) are calculated on the residuals, we suggest using correlation between residual patterns to define the clusters. For this data set, the same clusters resulted in either case.

We calculate the functional depth of each booking pattern and compute the threshold as described in Section 2.2. We then transform the depths as per equation (3) to obtain z_{nl} , as shown in Figure 9. The sums of threshold exceedances, z_n , were shown earlier in Figure 3, with the empirical distribution and fitted generalised Pareto distribution shown in Figures 4a and 4b, respectively.

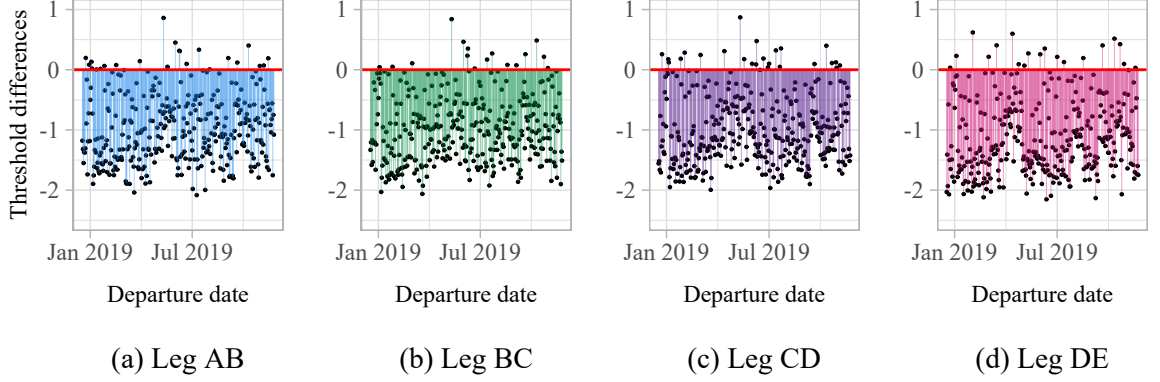


Figure 9: Threshold exceedances per leg, z_{nl}

Figure 10 highlights the outliers detected in each leg in pink, while depicting outliers detected in other legs but *not* in that leg in blue. Regular patterns are grey.

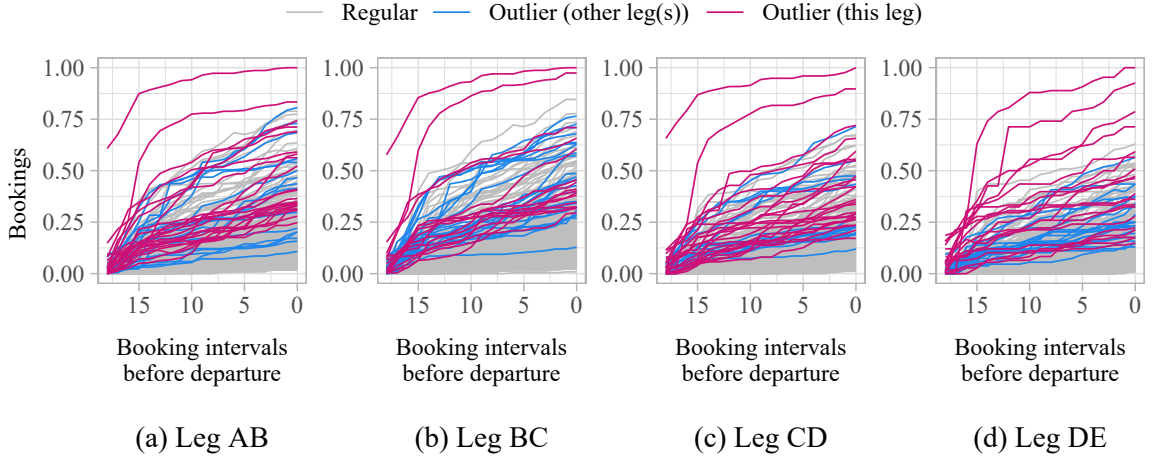


Figure 10: Outliers detected in booking patterns

Of the 40 outliers (11% of departures) detected across all legs, 23 outliers (almost 60%) could be attributed to known events or holidays. When considering only the top 10 outliers, the percentage rose to 70%. A further departure detected as an outlier had been previously flagged by Deutsche Bahn. The firm implemented a booking stop to control sales on that departure for multiple connected legs. Appendix B.5 provides further details on the distribution of identified outliers across

legs.

4 Computational Study: Settings

We implement a simulation model to evaluate the performance of outlier detection across a cluster of legs and stations. The simulation can evaluate revenue implications of adjusting the forecast by implementing network RM with capacity controls, which transforms simulated demand into booking observations. By varying demand for itineraries, we create outliers that are observable on both the leg and network level. As outliers are deliberately generated, we can evaluate detection quality on either level.

In this section we outline the simulation model, the choices of parameter values, and the setup of the computational experiments. The results of these experiments are documented in Section 5.

The simulation models a network consisting of 5 stations and 4 legs, mirroring the structure of the Deutsche Bahn network studied in Figure 7. There are ten possible itineraries represented by set $\mathcal{O} = \{AB, AC, AD, AE, BC, BD, BE, CD, CE, DE\}$. On each itinerary, the firm offers seven fare classes. We consider differentiated demand from two customer types represented by the set $\mathcal{I} = \{1, 2\}$.

4.1 Network revenue management system

The basic RM system optimises the set of offered fare classes not just per leg of the network, but by itinerary. To that end, a dynamic program computes bid prices on the leg-level, which are summed up to control offers on the itinerary-level – compare Strauss et al. (2018) and Appendix C.1 for technical details. The bid price describes the marginal difference between the value of selling a seat in the current time period and that of reserving it to sell in a future time period. The RM system only offers fare classes where the revenue from a booking exceeds the bid price. Bid prices are computed per leg of a network and depend on time until departure, unsold capacity, and expected demand. Booking patterns result from combining customer requests with the set of offered fare classes to generate bookings. Booking patterns are not reported for each individual itinerary, but only on the leg level.

Parameterising the dynamic program that computes bid prices requires predicting the expected demand arrival rates per leg l , fare class j , and time slice t of the booking horizon. Given that we know the underlying demand model for each itinerary, we can estimate the arrival rates for each leg l and fare class j by:

$$\hat{\Lambda}_{j,l}(t) = \sum_{o \in \mathcal{O}_l} \sum_{i \in \mathcal{I}} p_{i,j,o} \lambda_{i,o}(t), \quad (9)$$

where $\lambda_{i,o}(t)$ is the arrival rate of customers of type i requesting itinerary o , and \mathcal{O}_l is the set of itineraries which include leg l . This creates an artificially accurate demand forecast. Deriving the demand forecast from the actual demand parameter values ensures that the estimation of revenue loss caused by undetected outliers is not affected by flawed forecasts (see Section 5.2). In practice, demand parameter values are not known but are estimated based on previously observed demand and time series forecasting.

4.2 Demand settings

The simulation generates booking requests per customer type i according to a non-homogeneous Poisson process, where the arrival rate per itinerary o , $\lambda_{i,o}(t)$, at time t , is given by:

$$\lambda_{i,o}(t)|(D_o = d_o) = d_o \times \phi_{io} \frac{t^{a_{io}-1}(1-t)^{b_{io}-1}}{B(a_{io}, b_{io})}. \quad (10)$$

Here, ϕ_{io} is the fraction of customers of type i and $D_o \sim \text{Gamma}(\alpha_o, \beta_o)$ with probability density function:

$$f(d_o|\alpha_o, \beta_o) = \frac{\beta_o^{\alpha_o}}{\Gamma(\alpha_o) d_o^{\alpha_o-1} e^{\beta_o d_o}}. \quad (11)$$

We generate demand over a horizon of 3,600 time slices to ensure $\lambda_{io}(t) < 1$. This level of detail is required to accurately parameterise the dynamic program for bid price control. The resulting bookings are aggregated into 18 booking intervals.

Next, we define p_{ijo} as the probability that a customer of type i pays up to fare class j on itinerary o . We assume that customers book the cheapest available fare class. Combining this demand model with the four-leg-network creates 210 demand parameters. We set the parameters to mirror common RM assumptions (Weatherford and Bodily, 1992): (i) valuable customers from type 1 book later than customers from type 2, (ii) customers book earlier for longer journeys, and (iii) customers are willing to pay a higher fare class if they are travelling further. The majority of passengers book tickets boarding at A and leaving at E; this ensures the correlation between the legs exceeds 0.5 and guarantees that the legs are correctly modelled in the same cluster. As detailed in Appendix C.3, we validated that the functional dynamical correlation between the four legs for simulated data is comparable to the Deutsche Bahn data. Appendix C.3 also compares the simulated and empirical booking patterns to validate parameter choices.

We generate all regular demand as described above. The full list of parameter values can be found in Appendix C.2, Table 3. The simulation excludes trend and seasonality to evaluate outlier detection approaches in a best-case-scenario. In other

words, if an algorithm fails on observations from stationary demand, it will likely not perform better given more demand variability.

4.3 Outlier generation and evaluation

We focus on demand volume outliers, which we generate by changing the parameters of the Gamma distribution which governs the level of total demand (see equations (10) and (11)). We evaluate twelve shifts in the distributions, changing the mean by $\pm 10\%$, $\pm 20\%$, $\pm 30\%$, $\pm 40\%$, $\pm 50\%$, and $\pm 60\%$. For every shift in mean, we reduce demand variance by 80% to ensure a sufficiently outlying demand value.

We generate booking patterns for 500 departures, with 1% of departures affected by outlier demand. Previous work found the proportion of outliers had little effect on outlier detection performance in the single-leg case (Rennie et al., 2021).

We differentiate outlier scenarios in terms of the affected network components. Firstly, we evaluate a scenario where outlier demand affects all network itineraries. We consider the case where each outlier is randomly drawn from one of the twelve outlier distributions, resulting in outliers from a mixture of different distributions. This lets us test whether the ranking of the alert list mirrors the outliers' underlying degree of demand deviation. We then considers each of the twelve outlier distributions in isolation to assess the sensitivity of detection. Secondly, we evaluate a scenario where outliers only affect a single itinerary. This evaluates the benefits of clustering multiple legs. Appendix D.2.4 considers the practically relevant case of outliers affecting a subset of itineraries. The full extent of simulation experiments is shown in Appendix C.2.1.

Each combination of outcomes can be classified into one of four categories: (i) assigning a non-zero outlier severity to a genuine outlier creates a true positive (TP); (ii) assigning a zero outlier severity to a regular observation creates a true negative (TN); (iii) assigning a non-zero outlier severity to a regular observation creates a false positive (FP); (iv) assigning a zero outlier severity to a genuine outlier creates a false negative (FN). This classification enables us to compute the true positive rate (TPR) for the top R ranked departures in the alert list:

$$TPR_R = \frac{TP_R}{TP + FN}, \quad (12)$$

where TP_R is the number of true positives in the top R departures. The true positive rate lies between 0 and 1, where 1 means all genuine outliers were identified. We evaluate performance across 1,000 stochastic simulations.

To evaluate the effect of ranking outliers, we consider the increase in precision when the ranking is taken into account. For example, we consider the precision

in the top 5 ranked departures, versus 5 randomly chosen departures with non-zero outlier probabilities. The change in precision when considering the top R departures, $\Delta(Precision)_R$, is given by:

$$\Delta(Precision)_R = \frac{TP_R}{TP_R + FP_R} - \frac{TP_{R(random)}}{TP_{R(random)} + FP_{R(random)}}, \quad (13)$$

where $TP_{R(random)}$ is the number of true positives in a random selection of R departures with non-zero severity, and $FP_{R(random)}$ is defined analogously for false positives.

4.4 Forecast adjustments for outlier demand

The aim of identifying outlier demand in RM systems is to support analyst interventions. This raises the difficult question of predicting the consequences from analyst adjustments throughout the network. As a step in this direction, we analyse a best-case-scenario, assuming that the adjustment is made with foresight, before the start of the booking horizon. We compare the revenue under three different types of adjustment:

- **Adjustment 1 (conservative):** Adjust only forecasts of affected single-leg itineraries. E.g., for an outlier creating additional demand for itinerary AC, increase the forecasts of itineraries AB and BC.
- **Adjustment 2 (aggressive):** Adjust forecasts of itineraries that include at least one of the affected legs. E.g., for additional demand for itinerary AC, adjust all itineraries including either leg AB or leg BC – i.e., itineraries AB, AC, AD, AE, BC, BD, and BE.
- **Adjustment 3 (balanced):** Adjust forecasts of affected single-leg itineraries and the *cluster-spanning* itinerary – in this case, AE. E.g., for additional demand for itinerary AC, adjust itineraries AB, BC, and AE. The motivation for adjusting AE (ahead of other itineraries) is that in general this will be the most popular itinerary in the cluster.

As a lower bound, we compute the revenue when **no adjustment** is made. As an upper bound, we implement an **oracle adjustment**, i.e., only adjusting the forecasts of affected itineraries. We compare the revenue as the level of outlier demand ranges from -60% to +60% of the average leg level demand.

5 Computational Study: Results

5.1 Detecting outliers in multiple legs

First, we consider the scenario where outlier demand equally affects all itineraries and legs within the cluster. For this scenario, Figure 11a illustrates how the true positive rate (TPR) increases when increasing the length of alert list. In this figure, the red line indicates the number of genuine outliers. The true positive rates are promising, with a TPR of around 0.2 for a list length of 1. Since there are five genuine outliers, this indicates that a genuine outlier is almost always ranked top.

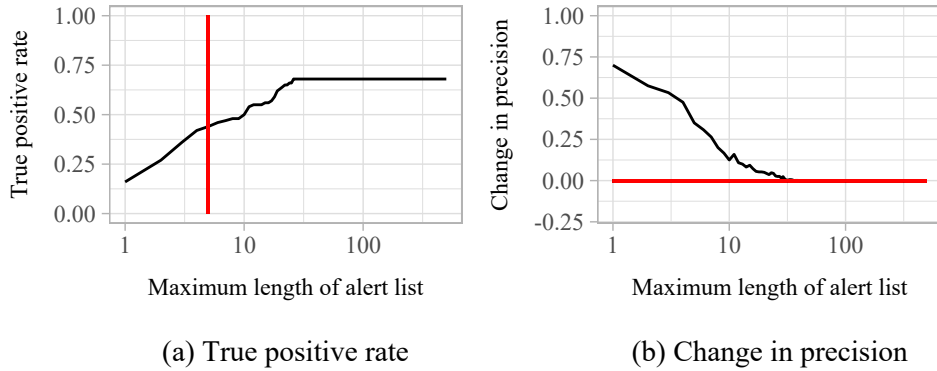


Figure 11: Performance for demand-volume outliers in all itineraries

Figure 11b highlights how the precision improves when ranking outliers as opposed to listing them in random order. Ranking particularly improves precision when the alert list covers less than 1% of all 500 departures. As domain experts indicate that analysts cannot target 1% or more of departures, ranking focuses resources and thereby provides large benefits in practice. Nevertheless, Figure 11 also highlights the trade-off between reducing the number of false alerts and identifying all outliers. A shorter length of alert list increases precision, but reduces the true positive rate.

In an ideal setting, the alert list should feature, from top to bottom, large outliers and subsequently smaller outliers. Figure 12 shows the distribution of each magnitude of outlier in the alert lists. The modes of the distributions generally fall where they should, as larger outliers are ranked higher. The smaller variance in the ranking of the larger magnitude outliers indicates that they are easier to detect. The higher variance of the medium sized outliers can be explained as the ranking of a medium sized outlier is dependent on which other types of outliers occur: if there is a large and a medium outlier, the medium outlier is ranked lower; if there is a small and a medium outlier, the medium outlier is ranked higher. Appendix

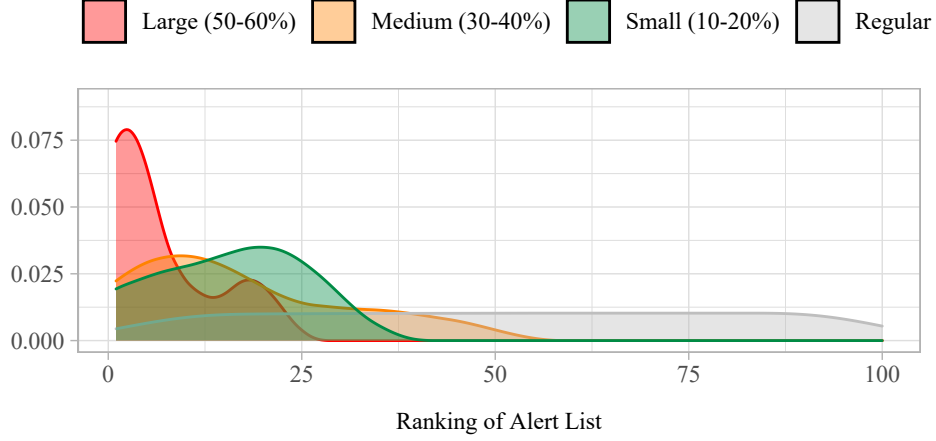


Figure 12: Distribution of outliers in ranked alert list

D.2.1 further analyses the distribution of identified outliers across different legs.

To better understand outlier detection performance, we break down the results by magnitude of outliers in Figure 13. When outliers are generated by minor changes

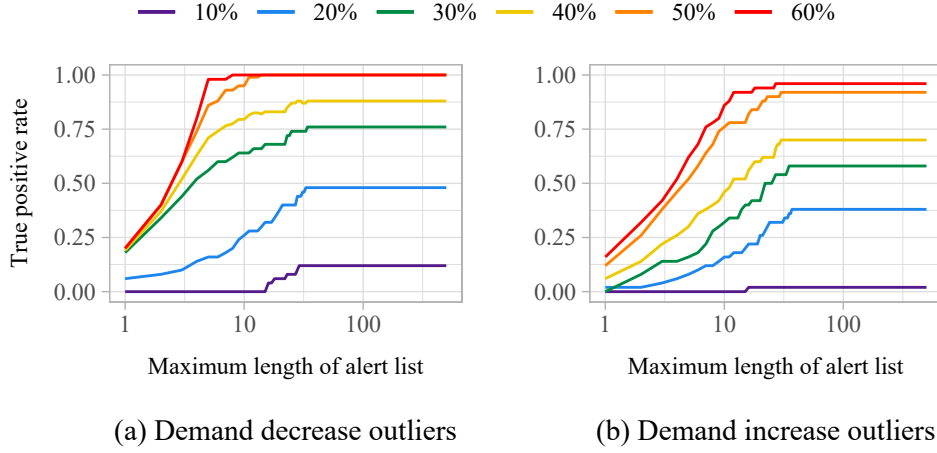


Figure 13: True positive rate for homogeneous demand-volume outliers by magnitude

in demand levels, they are difficult to detect, resulting in low true positive rates. Given the significant overlap between the distribution of outlier demand with a 10% change in magnitude and that of regular demand, this is to be expected. Therefore, 10% demand changes effectively provide a lower bound on how big an outlier needs to be in order to be detected.

As the magnitude of the outliers increases, they become easier to detect and true positive rates are higher, with peak rates reached with shorter alert lists. Thus,

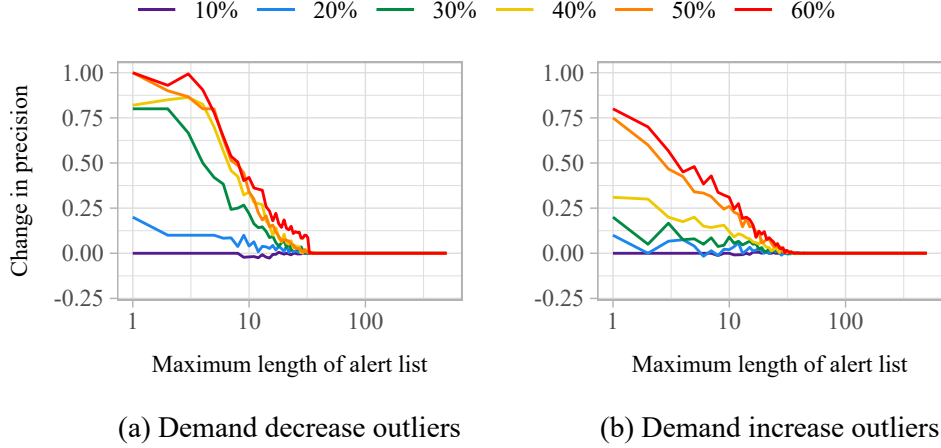


Figure 14: Increase in precision for homogeneous demand-volume outliers by magnitude

genuine outliers are more likely to be ranked higher when they are caused by larger demand changes. For demand decreases of at least 50%, the true positive rate is very close to the optimal detection rate. Negative demand outliers are slightly easier to detect than positive demand outliers, meaning shorter alert lists are required. This is due to the demand censoring imposed by the booking controls and capacity restrictions.

Figure 14 shows the precision gap over randomly ordered lists. Once more, larger magnitude outliers result in larger precision improvements from ranking, while detecting minor outliers gains little over random selection. Similarly, we observe that detecting negative demand outliers gains slightly more precision in comparison to detecting positive outliers of the same magnitude. Additional results regarding false discovery rates are available in Appendix D.2.2. In a second set of experiments, we analyse detection performance by breaking down results in terms of which itinerary the outlier demand is generated in. Figure 15 shows the true positive rate when outlier detection is performed just on the leg-level versus in the proposed aggregated manner. Here, we consider outlier demand generated by a 50% increase in the affected legs as an illustrative example. We show only the results relating to itineraries AB, AC, AD, and AE. Figure 30 in Appendix D.2.3 details results for the further itineraries yielding similar conclusions. For results when outlier demand is generated across combinations of itineraries, see Appendix D.2.4.

In all cases, the true positive rate for clusters is higher than in any of the individual legs. This is because when considering the leg's bookings in isolation for

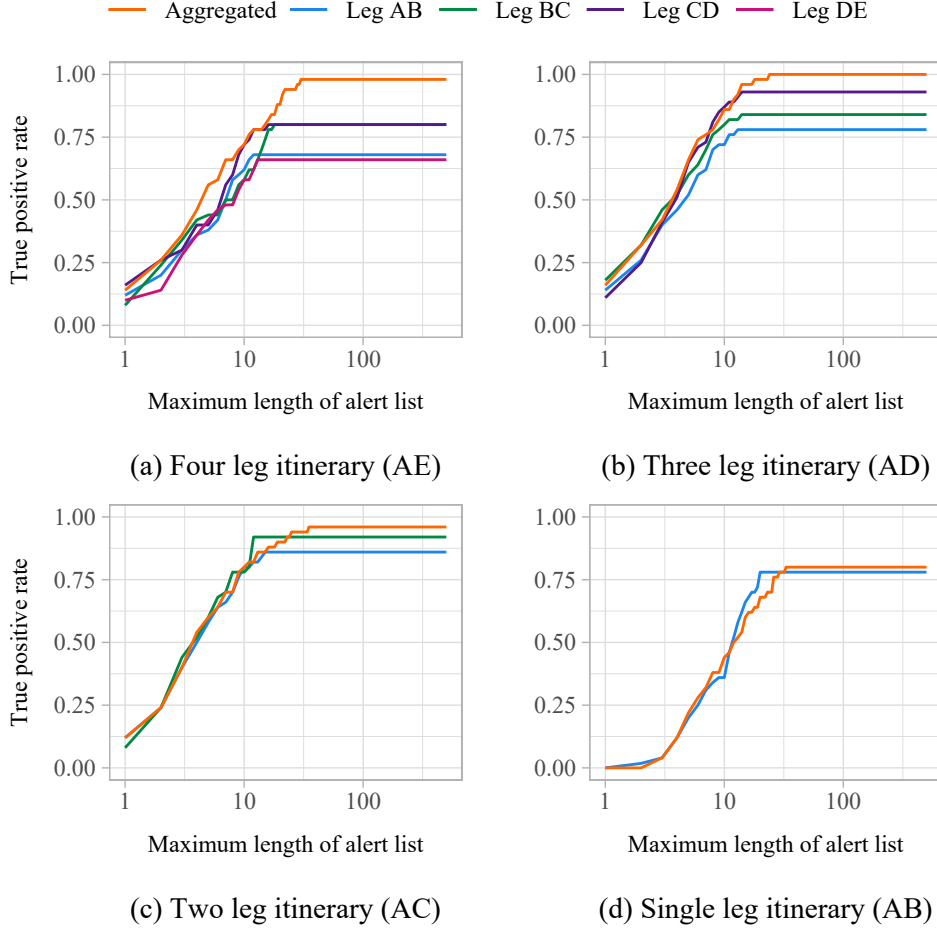


Figure 15: True positive rate for single itinerary outliers

outlier demand that affects multiple legs, the noise from other itineraries prevents detecting the outlier in every leg. However, clustering increases the number of detected genuine outliers.

Clustering is most beneficial when the outlier demand affects the most legs i.e. itinerary AE, as shown in Figure 15a. The lower true positive rates in legs AB and DE are due to different combinations of itineraries also utilising these legs. The aggregation is less beneficial when outlier demand affects an itinerary consisting of only one or two legs, since we aggregate the analysis across legs that are actually not affected by outlier demand. However, there is a modest gain in true positive rate even in this case. This is due to the knock-on effects of decreased capacity on the affected legs, impacting the bid prices for any itineraries which include these legs. For some lengths of alert list, the leg-level true positive rates are higher than the aggregated approach, due to false positives from unaffected legs being included in the list. However, even for itinerary AB (Figure 15d), where false positives from

unaffected legs are most likely, the difference is small and cancelled out by the overall increase in true positive rate.

5.2 Revenue benefits from forecast adjustments for outlier demand

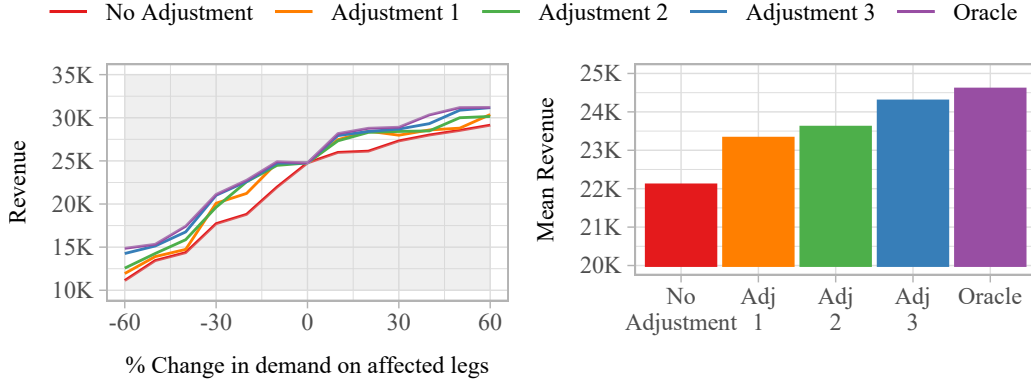
Figure 16 shows the revenue generated by outlier demand for each of the three possible choices of adjustment described in Section 4.4. We show the results for four of ten itineraries contained within these four legs. The results for the other six itineraries are similar to those presented here for the same corresponding leg length. Appendix D.3 details these results as well as further results on adjustments after outlier detection.

When outlier demand affects all four legs in the cluster (Figure 16a), any type of adjustment is always better than no adjustment. Besides the oracle, the best choice is adjustment 3, i.e., the balanced approach where the forecasts of the cluster-spanning itinerary and the individual leg are adjusted. Adjustment 3 is able to obtain, on average, 87% of the additional revenue gained under the oracle adjustment. Similar results are obtained when the outlier demand affects three legs (Figure 16b).

When outlier demand affects only a single-leg itinerary (Figure 16d), adjustment 1 (the conservative adjustment) and the oracle adjustment coincide. The aggressive approach of making an adjustment to all itineraries which include the affected leg yields less revenue than no adjustment. For example, although leg AB is correctly adjusted, the erroneous adjustment to itineraries AC, AD, and AE results in incorrect forecasts for legs BC, CD, and DE. The asymmetry between adjustment to positive and negative outlier demand is due to the level of demand being bounded below by 0.

Similar results emerge when the outlier affects only two of the affected legs (Figure 16c), though the negative consequences of over-adjusting all potentially affected itineraries are less severe, as this causes fewer superfluous adjustments.

The negative impact of adjusting unaffected itineraries highlights the importance of correctly clustering legs ahead of outlier detection. The closer the outlier demand itinerary is to the cluster spanning itinerary, the less risky it is to adjust all affected itineraries within a cluster, and the more benefit can be gained from doing so. From a managerial perspective, the *best* adjustment (other than the oracle) depends on the transport provider’s objective. To maximise revenue when the most common outlier (e.g. itinerary AE) occurs, the conservative approach of adjustment 3 is preferable. Conversely, if the objective is to minimise risk to revenue even in the more unlikely scenarios (e.g. an outlier in itinerary AB), adjustment 1 should



(a) Four leg itinerary (AE): revenue by demand change (left), mean revenue (right)

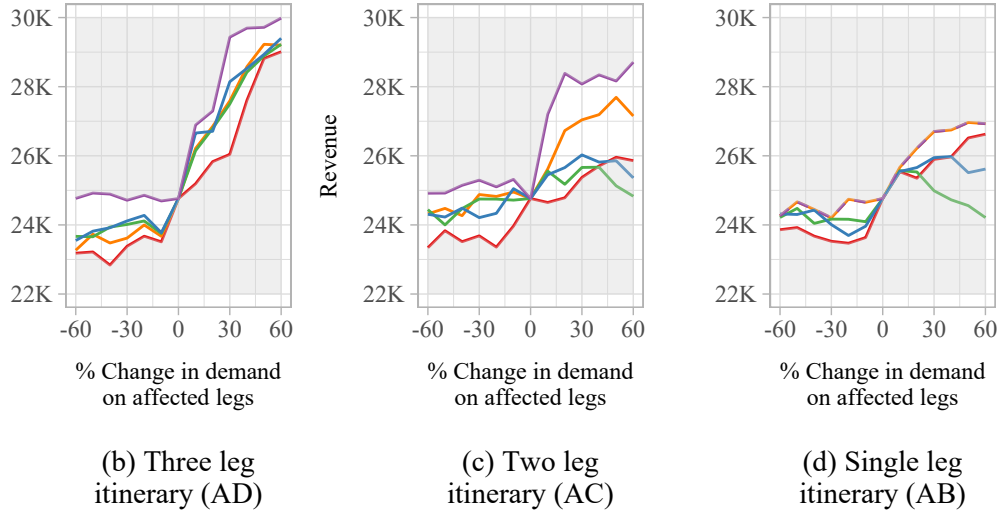


Figure 16: Revenue generated under different itinerary-level forecast adjustments, where the subtitle indicates the location of the outlier

be preferred. Overall, however, there are clear benefits from forecast adjustment.

6 Conclusion and outlook

In this paper, we proposed a two-step method for (i) identifying which legs in a mobility network are likely to benefit from joint outlier detection, and (ii) detecting outlying demand within such a set of legs. Furthermore, we presented an approach to rank identified outliers according to their severity, creating an alert list to aid analysts in prioritising demand forecast adjustments. By applying the proposed approach to empirical booking data, we demonstrated the type of data observed in practice and showed how to account for additional practical considerations, such

as trend and seasonality. Based on insights from analysing empirical data, we constructed a simulation to evaluate how successfully our method detects outliers under laboratory conditions.

The simulation study demonstrated the robustness of the method in a range of outlier demand scenarios. It highlighted that aggregating the analysis across clustered legs that share common outliers improves both detection rate and precision. Further, the ranked alert list correctly identified the most critical outliers. Last but not least, we measured the potential revenue benefits of identifying and adjusting for demand outliers in a network setting by applying a choice of forecast adjustments and gauging the resulting revenue. We show that taking into account the similarity of the legs can improve revenue in most scenarios. In the less likely scenario where only one or two legs of a cluster are affected by outlier demand, risk-averse firms may prefer leg-level adjustments.

Further research is needed to consider the practical aspects of outlier detection in live revenue management systems from the perspective of decision support. Such research should particularly focus on effective ways to visualise outliers in networks and to communicate the ranked alert list to RM analysts. Another research opportunity would be to consider how the aggregated outlier detection may be adapted for other areas of revenue management, e.g., in hotels, where correlation is induced by bookings for multiple consecutive nights. Similarly, investigating the use of alternative clustering approaches is of interest - particularly where the clusters are likely to be of different structures compared to the rail industry e.g. in the airline industry where hub and spoke networks are more common than lines.

Acknowledgements

We gratefully acknowledge the support of the Engineering and Physical Sciences Research Council funded EP/L015692/1 STOR-i Centre for Doctoral Training. The authors acknowledge Deutsche Bahn for the provision of data, and are grateful to Philipp Bartke and Valentin Wagner for helpful discussions and suggestions.

References

- Amelio, A. and Pizzuti, C. (2015). Is normalized mutual information a fair measure for comparing community detection methods? *Proceedings of the 2015 IEEE/ACM International Conference on Advances in Social Networks Analysis and Mining, ASONAM 2015*, pages 1584–1585.

- Augustin, K., Gerike, R., Martinez Sanchez, M. J., and Ayala, C. (2014). Analysis of intercity bus markets on long distances in an established and a young market: The example of the U.S. and Germany. *Research in Transportation Economics*, 48:245–254.
- Barrow, D. and Kourentzes, N. (2018). The impact of special days in call arrivals forecasting: A neural network approach to modelling special days. *European Journal of Operational Research*, 264(3):967–977.
- Currie, C. S. M. and Rowley, I. T. (2010). Consumer behaviour and sales forecast accuracy: what’s going on and how should revenue managers respond? *Journal of Revenue and Pricing Management*, 9:374–376.
- De Baets, S. and Harvey, N. (2020). Using judgment to select and adjust forecasts from statistical models. *European Journal of Operational Research*, 284(3):882–895.
- Dubin, J. A. and Müller, H. G. (2005). Dynamical correlation for multivariate longitudinal data. *Journal of the American Statistical Association*, 100:872–881.
- Fawcett, L. and Walshaw, D. (2007). Improved estimation for temporally clustered extremes. *Environmetrics*, 18(2):173–188.
- Fawzy, A., Mokhtar, H. M., and Hegazy, O. (2013). Outliers detection and classification in wireless sensor networks. *Egyptian Informatics Journal*, 14(2):157–164.
- Febrero, M., Galeano, P., and González-Manteiga, W. (2008). Outlier detection in functional data by depth measures, with application to identify abnormal NOx levels. *Environmetrics*, 19(4):331–345.
- Grimshaw, S. D. (1993). Computing maximum likelihood estimates for the generalized pareto distribution. *Technometrics*, 35(2):185–191.
- He, G., Müller, H. G., and Wang, J. L. (2003). Functional canonical analysis for square integrable stochastic processes. *Journal of Multivariate Analysis*, 85(1):54–77.
- Hubert, M., Claeskens, G., De Ketelaere, B., and Vakili, K. (2012). A new depth-based approach for detecting outlying curves. In Colubi, A., Fokianos, K., Gonzalez-Rodriguez, G., and Kontoghiorghe, E., editors, *Proceedings of COMP-STAT 2012*, pages 329–340.
- Kendall, M. G. (1938). A new measure of rank correlation. *Biometrika*, 30:81–93.

- Klein, R., Koch, S., Steinhardt, C., and Strauss, A. K. (2020). A review of revenue management: Recent generalizations and advances in industry applications. *European Journal of Operational Research*, 284(2):397–412.
- Lawrence, M., Goodwin, P., O’Connor, M., and Onkal, D. (2006). Judgmental forecasting: A review of progress over the last 25 years. *International Journal of Forecasting*, 22(3):493–518.
- Leadbetter, M. (1991). On a basis for ‘Peaks over Threshold’ modeling. *Statistics and Probability Letters*, 12(4):357–362.
- Pearson, K. (1895). VII. Note on regression and inheritance in the case of two parents. *Proc. R. Soc. Lond.*, 58.
- Perera, H. N., Hurley, J., Fahimnia, B., and Reisi, M. (2019). The human factor in supply chain forecasting: A systematic review. *European Journal of Operational Research*, 274(2):574–600.
- Pickands, J. (1975). Statistical Inference using Extreme Order Statistics. *The Annals of Statistics*, 3(1):119–131.
- Prim, R. (1957). Shortest connection networks and some generalizations. *Bell Systems Technology Journal*, 36:1389–1401.
- Ramsay, J. O. and Silverman, B. W. (1997). *Functional Data Analysis*. Springer, New York.
- Ranshous, S., Shen, S., Koutra, D., Harenberg, S., Faloutsos, C., and Samatova, N. F. (2015). Anomaly detection in dynamic networks: A survey. *WIRES: Computational Statistics*, 7(3):223–247.
- Rennie, N., Cleophas, C., Sykulski, A. M., and Dost, F. (2021). Identifying and responding to outlier demand in revenue management. *European Journal of Operational Research*.
- Ribatet, M. and Dutang, C. (2019). *POT: Generalized Pareto Distribution and Peaks Over Threshold*. R package version 1.1-7.
- Schaeffer, S. E. (2007). Graph clustering. *Computer Science Review*, 1(1):27–64.
- Schütze, C., Cleophas, C., and Tarafdar, M. (2020). Revenue management systems as symbiotic analytics systems: insights from a field study. *Business Research*, 13(3):1007–1031.

- Smith, R. L. (1985). Maximum Likelihood Estimation in a Class of Nonregular Cases. *Biometrika*, 72(1):67–90.
- Strauss, A. K., Klein, R., and Steinhardt, C. (2018). A review of choice-based revenue management: Theory and methods. *European Journal of Operational Research*, 271(2):375–387.
- Talluri, K. T. and Van Ryzin, G. J. (2004). *The Theory and Practice of Revenue Management*. Kluwer Academic Publishers.
- Weatherford, L. R. (2016). The history of forecasting models in revenue management. *Journal of Revenue and Pricing Management*, 15(3):212–221.
- Weatherford, L. R. and Belobaba, P. P. (2002). Revenue impacts of fare input and demand forecast accuracy in airline yield management. *The Journal of the Operational Research Society*, 53(8):811–821.
- Weatherford, L. R. and Bodily, S. E. (1992). A taxonomy and research overview of perishable-asset revenue management: Yield management, overbooking, and pricing. *Operations Research*, 40:831–844.
- Weatherford, L. R. and Kimes, S. E. (2003). A comparison of forecasting methods for hotel revenue management. *International Journal of Forecasting*, 19(3):401–415.
- Yuan, W., Nie, L., Wu, X., and Fu, H. (2018). A dynamic bid price approach for the seat inventory control problem in railway networks with consideration of passenger transfer. *PloS one*, 13(8):e0201718.
- Zahn, C. T. (1971). Graph-Theoretical Methods for Detecting and Describing Gestalt Clusters. *IEEE Transactions on Computers*, C-20(1):68–86.

Appendices

A Additional details of method

Appendix A provides additional details on the proposed method described in Section 2, including the specifics of the correlation-based minimum spanning tree clustering, and the calculation of the functional depths.

A.1 Functional dynamical correlation

Let $y_{n,ij}(t)$ be the total observed bookings for the n^{th} departure on leg ij up to booking interval t , and similarly for $y_{n,jk}(t)$. The functional dynamical correlation between the booking patterns $y_{n,ij}(t)$ and $y_{n,jk}(t)$ is:

$$\rho_n(ij, jk) = \mathbb{E}\langle y_{n,ij}^*(t), y_{n,jk}^*(t) \rangle. \quad (14)$$

where

$$\langle y_{n,ij}^*(t), y_{n,jk}^*(t) \rangle = \int y_{n,ij}^*(t) y_{n,jk}^*(t) w(t) dt, \quad (15)$$

and $w(t)$ is a weight function that accounts for the time gap between observations. Here, $y_{n,ij}^*(t)$ is a standardised version of $y_{n,ij}(t)$:

$$y_{n,ij}^*(t) = \frac{y_{n,ij}(t) - M_{ij} - \mu_{ij}(t)}{\left[\int \{y_{n,ij}(t) - M_{ij} - \mu_{ij}(t)\}^2 w(t) dt \right]^{1/2}}, \quad (16)$$

where $\mu_{ij}(t)$ is a mean function, and:

$$M_{ij} = \langle y_{n,ij}(t), 1 \rangle. \quad (17)$$

The functional dynamical correlation is then the average across all N departures:

$$\rho(ij, jk) = \frac{1}{N} \sum_{n=1}^N \rho_n(ij, jk). \quad (18)$$

A.2 Prim's algorithm

Prim's algorithm is a greedy algorithm with the following basic steps. Assuming the original graph G has $V(G)$ vertices.

- Initialise the MST, T , with the edge with minimum weight and the two vertices it connects. Let $V(T)$ be the number of edges in T .
- While $V(T) < V(G)$:
 - go through the remaining edges in G in order from smallest to largest weights, until one is found that is connected to T , but does not form a circuit (i.e. the edge does not form a loop such that T is no longer a tree).
 - Add this edge (and the vertices it connects) to T .

More computationally efficient algorithms exist but given the reasonable size of the graphs considered, and more specifically their sparsity (very few stations are adjacent), computational time is reasonable using Prim's algorithm.

A.3 Functional depth

The functional halfspace depth is given by:

$$d_{nl}(\mathbf{y}_{nl} \in \mathcal{Y}_l; \alpha) = \sum_{j=1}^T w_\alpha(t_j) HD_j(\mathbf{y}_{nl}(t_j)), \quad (19)$$

where, using $t_{\tau+1} = t_\tau + 0.5(t_\tau - t_{\tau-1})$, the weights $w_\alpha(t_j)$ are, according to Hubert et al. (2012):

$$w_\alpha(t_j) = \frac{(t_{j+1} - t_j) \text{vol} [\{\mathbf{x} \in \mathbb{R}^k : HD_j(\mathbf{x}) \geq \alpha\}]}{\sum_{j=1}^T (t_{j+1} - t_j) \text{vol} [\{\mathbf{x} \in \mathbb{R}^k : HD_j(\mathbf{x}) \geq \alpha\}]}, \quad (20)$$

where $\alpha \in (0, 0.5]$, with a default value of $\alpha = 1/T$. The sample halfspace depth of a K -variate vector x at time t_j is given by (Hubert et al., 2012):

$$HD_j(y_{nl}(t_j)) = \frac{1}{N} \min_{\mathbf{u}, \|\mathbf{u}\|=1} \# \{y_{nl}(t_j), n = 1, \dots, N : \mathbf{u}^T y_{nl}(t_j) \geq \mathbf{u}^T \mathbf{x}\} \quad (21)$$

A.4 Normalised Mutual Information

For a graph containing M legs, the mutual information between two clusterings \mathcal{A} and \mathcal{B} of the M nodes in the inverted graph is defined as:

$$I(\mathcal{A}, \mathcal{B}) = \sum_{a=1}^{|\mathcal{A}|} \sum_{b=1}^{|\mathcal{B}|} \frac{|\mathcal{A} \cap \mathcal{B}|}{M} \log \left(|\mathcal{A} \cap \mathcal{B}| \frac{M}{M_a M_b} \right), \quad (22)$$

where M_a is the number of nodes in the a^{th} cluster of clustering \mathcal{A} , and similarly for M_b . The **normalised mutual information (NMI)** between two clusterings is defined as (Amelio and Pizzuti, 2015):

$$NMI(\mathcal{A}, \mathcal{B}) = \frac{2I(\mathcal{A}, \mathcal{B})}{H(\mathcal{A}) + H(\mathcal{B})}, \quad (23)$$

where $H(\mathcal{A})$ is the entropy (a measure of uncertainty) defined as:

$$H(\mathcal{A}) = - \sum_{a=1}^{|\mathcal{A}|} \frac{M_a}{M} \log \left(\frac{M_a}{M} \right). \quad (24)$$

$NMI(\mathcal{A}, \mathcal{B}) = 1$ if \mathcal{A} and \mathcal{B} are identical, and 0 if they are completely different.

B Empirical study of Deutsche Bahn booking data

Appendix B contains additional analysis of the empirical booking data from Deutsche Bahn, as described in Section 3.

B.1 Model selection for functional regression

Due to the functional nature of the data, in order to determine which of the factors result in a better fitting model, we use the **Cross-Validated Sum Of Integrated Squared Errors** (CV-SSE).

$$CV-SSE = \sum_{n=1}^N \int (y_{nl}(t) - \hat{y}_{nl}(t))dt, \quad (25)$$

where $\hat{y}_{nl}(t)$ is the prediction for the n^{th} booking pattern on the leg l , under the model fitted to all but the n^{th} booking pattern. The model which produces the lowest CV-SSE is chosen as the best fitting. Note that unlike other model selection criterion (e.g. AIC), CV-SSE does not take into account the number of parameters. Given that we are not interested in out of sample prediction, only in obtaining the best fitting model for our data, over-fitting is not of great concern. The values of the CV-SSE for each of the 12 models considered are shown in Table 2.

Model	Intercept	Day	Month	Short Horizon (I)	Short Horizon (C)	CV-SSE			
						Leg AB	Leg BC	Leg CD	Leg DE
Model 1	✓					79974160	75034839	79529280	73824611
Model 2	✓			✓		58617546	52622148	52424683	50009080
Model 3	✓				✓	58620898	52863263	52506946	50014984
Model 4	✓	✓				27227350	35376732	32789181	30037659
Model 5	✓	✓		✓		26551341	33724380	32282900	29989390
Model 6	✓	✓			✓	26704943	34154782	32439972	30019196
Model 7	✓		✓			58620649	57895619	52638923	50015645
Model 8	✓		✓	✓		58608640	57865403	52615801	49996331
Model 9	✓		✓		✓	58878374	57885484	52654330	50033157
Model 10	✓	✓	✓			24574978	25700166	21691111	21880038
Model 11	✓	✓	✓	✓		24519539	25691637	21689686	21878259
Model 12	✓	✓	✓		✓	24546715	25697938	21724073	21896889

Table 2: Model comparison for functional regression

Across all legs, we find that day, month, and shortened booking horizons are all factors that must be taken into account. The inclusion of the days of the week as factors significantly reduces the CV-SSE. In comparison, the inclusion of the booking horizon variable has a smaller, though still positive, effect. We compare two different approaches to accounting for the shortened booking horizon: (i) an indicator function (I) equal to 1 if the booking horizon is shorter, and (ii) a continuous variable (C) between 0 and 1 which gives the length of the shortened horizon as a proportion of the regular length horizon. Based on the CV-SSE scores, shortened booking horizons are best represented by the indicator function i.e. it is important to know that it is shorter but not by how much. The smaller effect of the horizon length variable may be related to the inclusion of the month variable, which is unsurprising given the overlap in the definition of these variables. The values of the

CV-SSE is similar for the models 2 and 7, where we only consider one of month or horizon length as a factor.

B.2 Residual booking patterns

Figure 17 shows the residual booking patterns resulting from the functional regression applied in equation (8) of Section 3.2. Compare with Figure 8 of Section 3.2 – the obvious outliers are preserved.

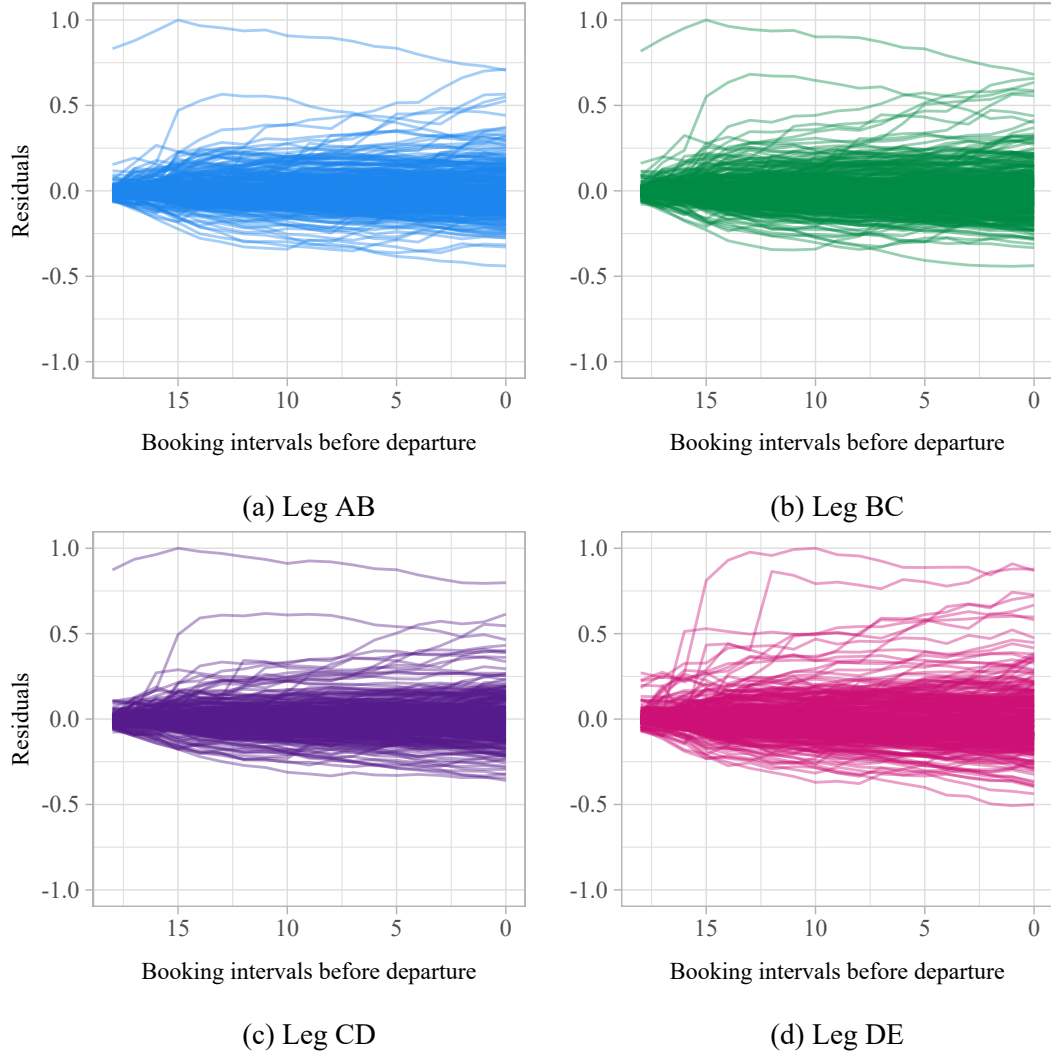


Figure 17: Residual booking patterns

B.3 Functional depths

Figure 18 shows the functional depths for the empirical residual booking patterns, before the functional depths are transformed into the z_{nl} , as shown in Figure 9 of Section 3.2.

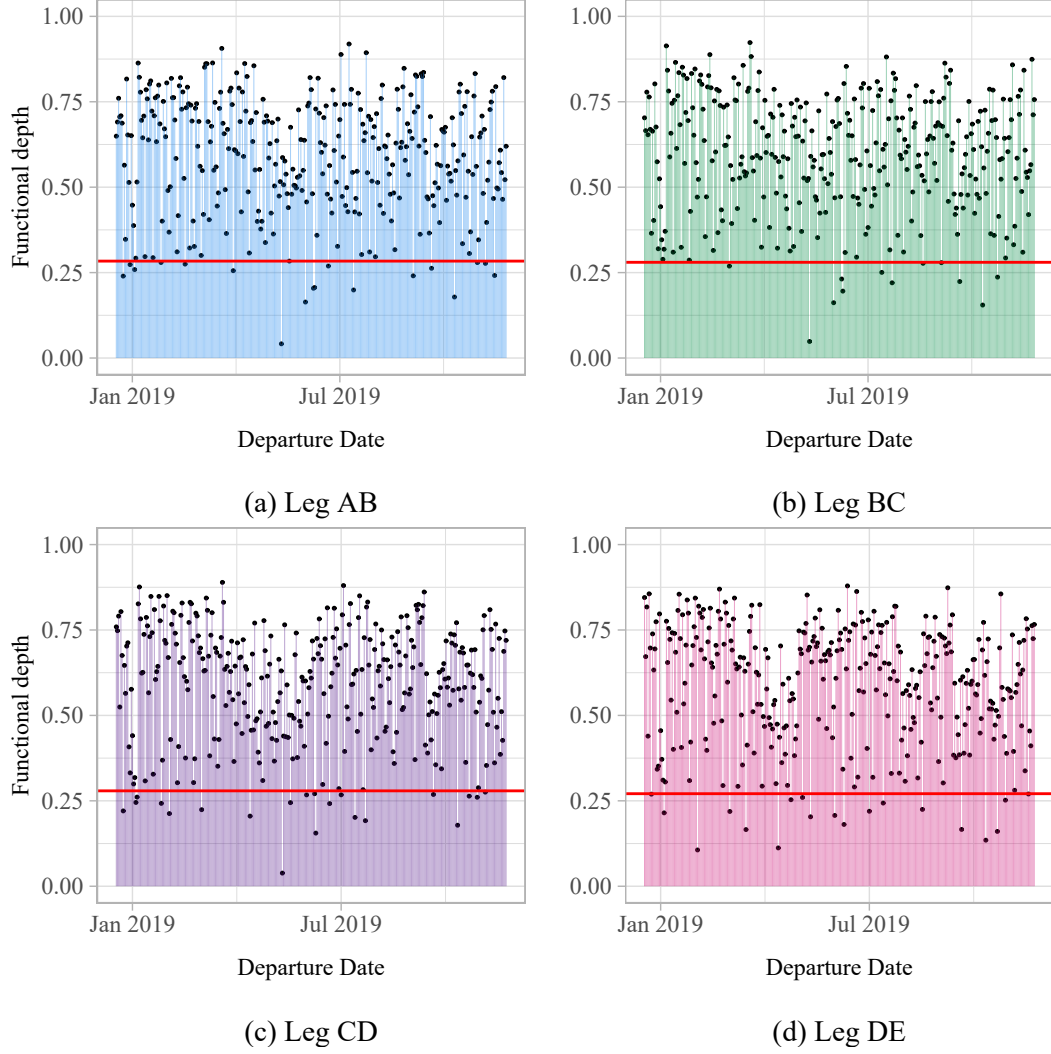


Figure 18: Functional depths

B.4 Probability plots for GPD and Exponential distributions

Given that, if both $\mu = 0$ and $\xi = 0$, the GPD reduces to an exponential distribution, it is appropriate to compare the fit of the GPD with an exponential distribution to check if the inclusion of additional parameters is beneficial. Figure 19 shows the P-P plots, i.e. the fitted theoretical CDF against the empirical CDF for the GPD (Figure 19a) and the Exponential distribution (Figure 19b). The GPD provides a closer fit to the empirical data and the additional parameters better account for the shape of the distribution. The GPD does not provide a perfect fit, with the

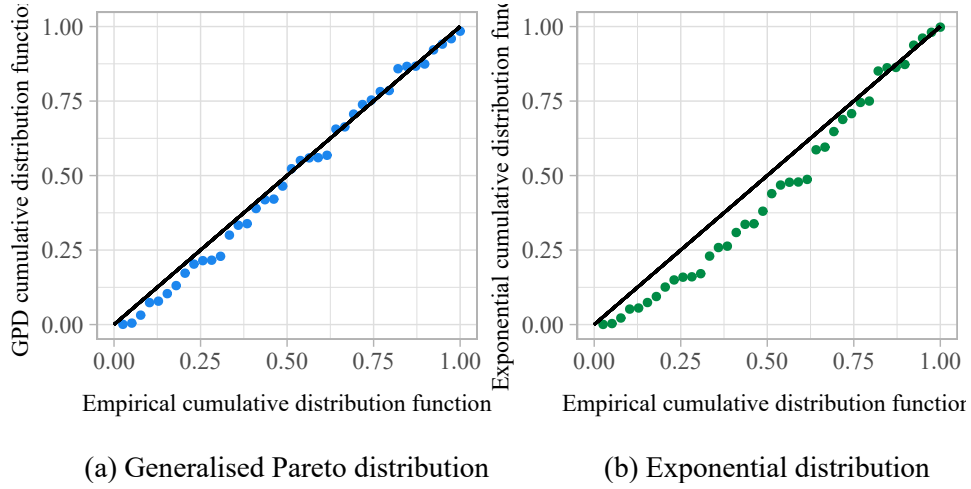


Figure 19: P-P plots

probabilities in the bottom left of Figure 19a on consistently being underestimated. However, given that we assume points with very low probability are more likely to be false positives, under-estimating may actually be beneficial. Further, only the highly-ranked outliers i.e. those with high probability, are likely to be considered by an analyst due to time-constraints. The GPD provides a very good fit for those data points. If there is a sufficiently large number of threshold exceedances, an empirical distribution could alternatively be used to compute the probabilities.

B.5 Distribution of outliers across multiple legs

The proportion of outliers found in each number of legs is shown in Figure 20, with over half of the outliers detected in multiple legs. Compared with Figure 26, this shows a similar proportion of outliers as found in the simulation study.

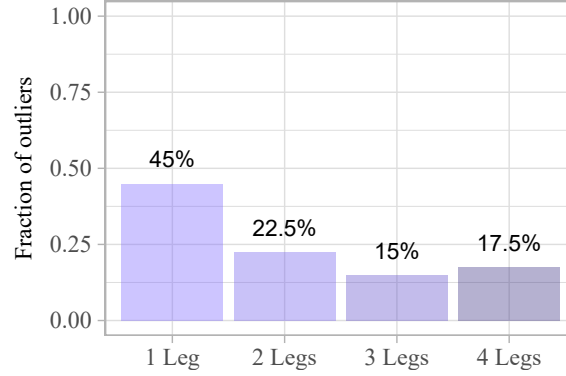


Figure 20: Fraction of all outliers detected in 1, 2, 3, or 4 legs

Figure 21a shows the proportion of total outlying booking patterns in terms of which legs they were detected as outliers in. Figure 21b shows the proportion in each leg of outlying booking patterns detected in one leg only. The proportions are fairly evenly split between the different legs. This reassures us that the correct clustering was chosen - if leg DE did in fact belong to a separate second cluster, we would expect a higher proportion of single leg outliers to have been found in leg DE – compare with Figure 27.

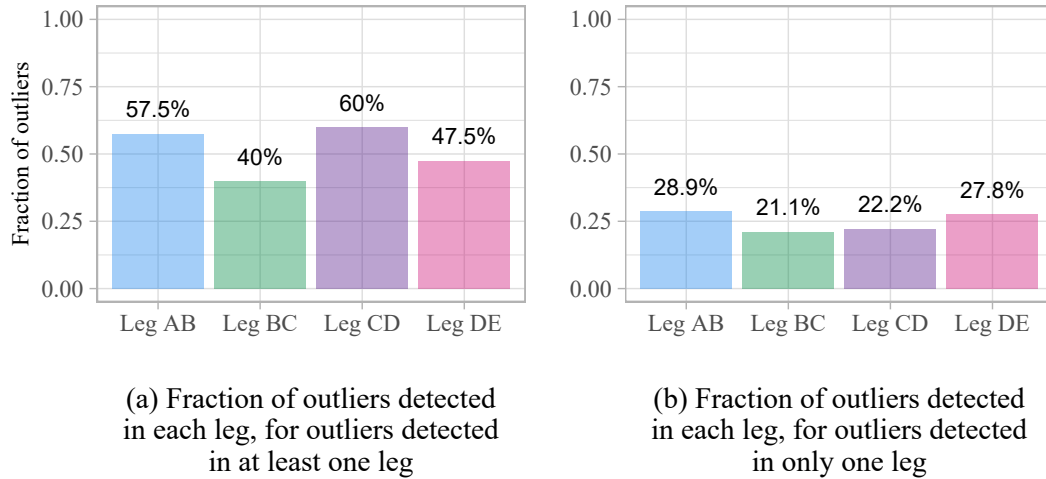


Figure 21: Fraction of outliers detected in each leg

C Details of computational study

Appendix C contains additional details of the simulation set up described in Section 4, including the computation of the bid prices, and a validation of the chosen parameter values.

C.1 Dynamic programming for bid price control

From Talluri and Van Ryzin (2004), let x be the remaining capacity, and define $V_t(x)$ denote the value function at time t . Define $R(t)$:

$$R(t) = \begin{cases} r_j & \text{if request for fare class } j \text{ arrives in interval } t \\ 0 & \text{otherwise} \end{cases} \quad (26)$$

where r_j denotes the revenue from accepting a request for fare class j . The probability that $R(t) = r_j$ is equal to the arrival rate for fare class j at time t . Note the arrival rates are such that at most one request arrives in each time period. Define:

$$u = \begin{cases} 1 & \text{if request for fare class } j \text{ arrives and is accepted} \\ 0 & \text{otherwise} \end{cases} \quad (27)$$

We wish to maximise the combined revenue in the current time period, and the revenue to come in future time periods:

$$\max_{u \in \{0,1\}} (R(t)u + V_{t+1}(x - u)) \quad (28)$$

The Bellman equation for $V_t(x)$ is:

$$V_t(x) = \mathbb{E} \left[\max_{u \in \{0,1\}} \{R(t)u + V_{t+1}(x - u)\} \right] \quad (29)$$

$$= V_{t+1}(x) + \mathbb{E} \left[\max_{u \in \{0,1\}} \{(R(t) + \Delta V_{t+1}(x))u\} \right] \quad (30)$$

$$V_t(x) = \sum_{j=1}^{|\mathcal{J}|} \lambda_j(t) \max \{ (r_j - \Delta V_{t+1}(x)), 0 \} \quad (31)$$

where $\lambda_j(t)$ is the arrival rate of demand for fare class j in interval t , and $\Delta V_{t+1}(x) = V_{t+1}(x) - V_{t+1}(x - 1)$ is the marginal cost of capacity in the next time period. The problem is solved with backwards recursion, with the following boundary conditions apply:

$$V_{T+1}(x) = 0, \quad x = 0, 1, \dots, C \quad (32)$$

$$V_t(0) = 0, \quad t = 1, \dots, T \quad (33)$$

These ensure (i) no revenue can be generated beyond the booking horizon i.e after departure; and (ii) that no further revenue can be generated if there is no capacity remaining. The bid price at time t with remaining capacity x is given by $\Delta V_t(x)$.

C.2 Parameter values for simulation study

Table 3: Regular demand generation parameter values

Parameter	Value	Effect of parameter
$\alpha = \{\alpha_{AB}, \alpha_{AC}, \alpha_{AD}, \alpha_{AE}, \alpha_{BC}, \alpha_{BD}, \alpha_{BE}, \alpha_{CD}, \alpha_{CE}, \alpha_{DE}\}$	$\alpha = \{32, 14, 14, 180, 4, 4, 14, 4, 14, 32\}$	Parameters of the Gamma distribution which controls the level of total demand across all fare classes and customer types such that the mean demand for itinerary o is: $\mathbb{E}(D_o) = \frac{\alpha_o}{\beta_o}$.
$\beta = \{\beta_{AB}, \beta_{AC}, \beta_{AD}, \beta_{AE}, \beta_{BC}, \beta_{BD}, \beta_{BE}, \beta_{CD}, \beta_{CE}, \beta_{DE}\}$	$\beta = \{1, 1, 1, 1, 1, 1, 1, 1, 1, 1\}$	
$\mathbf{a}_1 = \{a_{1,AB}, a_{1,AC}, a_{1,AD}, a_{1,AE}, a_{1,BC}, a_{1,BD}, a_{1,BE}, a_{1,CD}, a_{1,CE}, a_{1,DE}\}$	$\mathbf{a}_1 = \{5, 5, 5, 5, 5, 5, 5, 5, 5, 5\}$	Parameters of Beta distribution which controls the arrival times of type 1 customers
$\mathbf{b}_1 = \{b_{1,AB}, b_{1,AC}, b_{1,AD}, b_{1,AE}, b_{1,BC}, b_{1,BD}, b_{1,BE}, b_{1,CD}, b_{1,CE}, b_{1,DE}\}$	$\mathbf{b}_1 = \{2, 2, 2, 2, 2, 2, 2, 2, 2, 2\}$	
$\mathbf{a}_2 = \{a_{2,AB}, a_{2,AC}, a_{2,AD}, a_{2,AE}, a_{2,BC}, a_{2,BD}, a_{2,BE}, a_{2,CD}, a_{2,CE}, a_{2,DE}\}$	$\mathbf{a}_2 = \{2, 2, 2, 2, 2, 2, 2, 2, 2, 2\}$	Parameters of Beta distribution which controls the arrival times of type 2 customers
$\mathbf{b}_2 = \{b_{2,AB}, b_{2,AC}, b_{2,AD}, b_{2,AE}, b_{2,BC}, b_{2,BD}, b_{2,BE}, b_{2,CD}, b_{2,CE}, b_{2,DE}\}$	$\mathbf{b}_2 = \{2, 3, 5, 7, 2, 3, 5, 2, 3, 2\}$	
$\mathbf{p}_{1jo} = \{p_{1Ao}, p_{1Oo}, p_{1Jo}, p_{1Po}, p_{1Ro}, p_{1So}, p_{1Mo}\}$	$\mathbf{p}_{1jo} = \{0.30, 0.25, 0.20, 0.15, 0.10, 0, 0\}$	Probability of purchase for each customer type. It is assumed these are constant across itineraries. The no-purchase probability for customer type i is equal to $1 - \sum_{j \in \mathcal{J}} p_{ijo}$.
$\mathbf{p}_{2jo} = \{p_{2Ao}, p_{2Oo}, p_{2Jo}, p_{2Po}, p_{2Ro}, p_{2So}, p_{2Mo}\}$	$\mathbf{p}_{2jo} = \{0, 0.05, 0.10, 0.15, 0.20, 0.25, 0.25\}$	

Parameter	Value	Effect of parameter
$\phi_o = \{\phi_{1,o}, \phi_{2,o}\}$	$\phi_o = \{0.5, 0.5\} \forall o$	Proportion of total demand from each customer type for each itinerary. It is assumed these are constant across itineraries.

C.2.1 Outliers considered in computational study

Table 4 shows the different experiments that were carried out as part of the computational study. We consider *cluster* outliers in which every itinerary within the cluster is equally affected; *itinerary* outliers where only a single itinerary within the cluster is affected; and *station* outliers which affect all itineraries that end at a particular station.

Experiment	Outlier Type	Itineraries Affected	Magnitudes
1	Cluster	All	+10%, +20%, +30%, +40%, +50%, +60%, -10%, -20%, -30%, -40%, -50%, -60%
2	Itinerary	AB	+50%
3		AC	+50%
4		AD	+50%
5		AE	+50%
6		BC	+50%
7		BD	+50%
8		BE	+50%
9		CD	+50%
10		CE	+50%
11		DE	+50%
12	Station	AB	+50%
13		AC, BC	+50%
14		AD, BD, CD	+50%
15		AE, BE, CE, DE	+50%

Table 4: Different types of outliers considered in computational study

C.3 Simulation verification

In order to validate the parameter choices used to simulate booking patterns, we compare the resulting simulated booking patterns with the empirical booking patterns. We consider the standard deviation and mean of the bookings across the booking horizon of each in Figure 22. Both the empirical and simulated booking patterns show a similar shape and magnitude of relationship between the mean and standard deviation across the booking horizon.

We also compare the correlations between the different legs for both the empirical and simulated data. Table 5 shows the functional dynamical correlation between

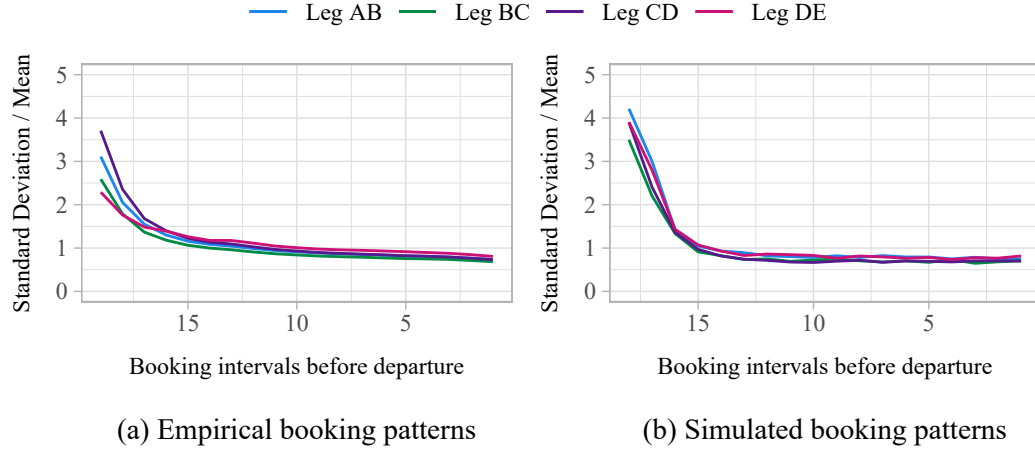


Figure 22: Comparison of standard deviation divided by mean of booking patterns

the empirical booking patterns, and empirical residual booking patterns, for each leg. Table 6 shows the corresponding correlations between the simulated booking patterns. The values are similar and the rate of decay between legs as they get further apart follows a similar pattern.

	Leg AB	Leg BC	Leg CD	Leg DE
Leg AB	-	0.95	0.83	0.70
Leg BC	-	-	0.83	0.66
Leg CD	-	-	-	0.78
Leg DE	-	-	-	-

(a) Booking patterns

	Leg AB	Leg BC	Leg CD	Leg DE
Leg AB	-	0.92	0.75	0.58
Leg BC	-	-	0.88	0.74
Leg CD	-	-	-	0.84
Leg DE	-	-	-	-

(b) Residual booking patterns

Table 5: Functional dynamical correlation of empirical booking patterns

	Leg AB	Leg BC	Leg CD	Leg DE
Leg AB	-	0.81	0.72	0.60
Leg BC	-	-	0.86	0.68
Leg CD	-	-	-	0.78
Leg DE	-	-	-	-

Table 6: Functional dynamical correlation of simulated booking patterns

D Computational results

Appendix D includes the extended results from the computational study described in Section 5. Results from additional simulation experiments to test the proposed clustering approach are also presented here.

D.1 Evaluation of network clustering

For the correlation-based clustering to perform well it needs to (i) accurately estimate similarity between adjacent legs, and (ii) use information about pairwise similarity between adjacent legs to detect similarity between (potentially) more than two legs to form clusters. We use the proportion of total demand belonging to each itinerary to determine a clustering benchmark. For example, in Figure 23a, when *all* passengers travel the itinerary from A to E, the resulting bookings in each of the four legs would be identical. In this case, the correlation between legs would be 1 – giving a single cluster of four legs.

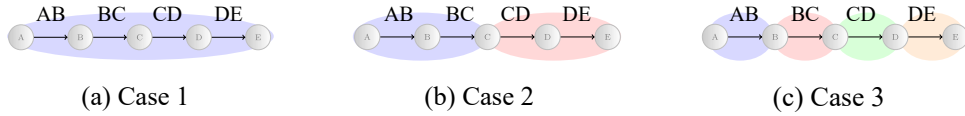


Figure 23: Benchmark clustering

We vary the level of demand for each itinerary to generate different benchmark clusterings. The output of the correlation-based clustering is then compared with benchmark clustering using the NMI. We consider three cases: the four legs belong in a single cluster (Figure 23a); they belong in two clusters (Figure 23b); and they belong in four clusters (Figure 23c).

- **Case 1:** When itinerary AE accounts for at least 50% of the network demand, we expect legs AB, BC, CD, and DE to belong to the same cluster, as they experience mostly the same demand. Remaining demand is calibrated across itineraries such that total demand for each leg is reasonably uniformly distributed. We compare the correlation-based clustering with the benchmark clustering of all four legs in a single cluster, when the average percentage of demand on each leg from itinerary AE is 50%, 60%, 70%, 80%, 90%, or 100%. Figure 24a shows the fraction of total demand on each leg, from each itinerary, in the case where 60% of demand is for itinerary AE.

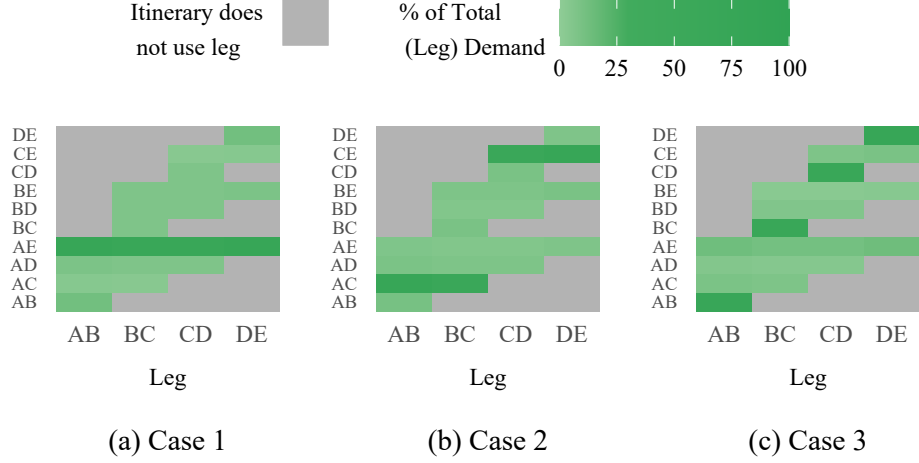


Figure 24: Itinerary demand per leg

- **Case 2:** We calibrate the majority of demand on leg AB and BC to be for itinerary AC, and the majority of demand on legs CD and DE to be demand for itinerary CE. For simplicity, the distribution of demand is symmetric across the four legs. We compare the performance when the average percentage of demand on each leg belonging to the clustering benchmark itinerary is 50%, 60%, 70%, 80%, 90%, or 100%. Figure 24b shows the case where 60% of demand on each leg is for the respective cluster itineraries (AC or CE).
- **Case 3:** We calibrate the majority of demand on leg AB for itinerary AB, the majority of demand on leg BC for itinerary BC, and so on. We compare the performance when the average percentage of demand on each leg belonging to the leg itinerary is 50%, 60%, 70%, 80%, 90%, or 100%. Figure 24c shows the case where 60% of demand on each leg is for the itinerary consisting of only that leg.

The results are shown in Table 7.

	Fraction of Leg Demand Resulting from Cluster Itinerary Demand					
	50%	60%	70%	80%	90%	100%
Case 1	0.99	1.00	1.00	1.00	1.00	1.00
Case 2	0.98	0.99	1.00	1.00	1.00	1.00
Case 3	0.94	0.97	0.99	1.00	1.00	1.00

Table 7: Normalised mutual information

In almost all cases, the normalised mutual information between the correlation-based clustering and the benchmark equals 1, indicating congruence. We now ex-

tend the simulation study by comparing the output of the correlation-based clustering under different correlation measures. In addition to the functional dynamical correlation measure described in Section 2.1, we compare *Pearson correlation* (Pearson, 1895) and *Kendall rank correlation* (Kendall, 1938). Let $y_{n,ij}(t)$ be the observed bookings for the n^{th} departure on leg ij , and $y_{n,pq}(t)$ analogous for leg pq .

- **Pearson correlation:** calculate the Pearson correlation between corresponding booking patterns, then average across all booking patterns. That is, for the n^{th} of N booking patterns observed over T booking intervals, we calculate the Pearson correlation coefficient as:

$$\rho_n(ij, pq) = \frac{\sum_{t=1}^T (y_{n,ij}(t) - \overline{y_{n,ij}})(y_{n,pq}(t) - \overline{y_{n,pq}})}{\sqrt{\sum_{t=1}^T (y_{n,ij}(t) - \overline{y_{n,ij}})^2} \sqrt{\sum_{t=1}^T (y_{n,pq}(t) - \overline{y_{n,pq}})^2}} \quad (34)$$

where $\overline{y_{n,ij}}$ is the mean number of bookings for the n^{th} booking pattern. Then:

$$\rho(ij, pq) = \frac{1}{N} \sum_{n=1}^N \rho_n(ij, pq). \quad (35)$$

- **Kendall rank correlation:** observations $(y_{n,ij}(s), y_{n,pq}(s))$ and $(y_{n,ij}(t), y_{n,pq}(t))$ where $s < t$, are *concordant* if their ordering agrees, and *discordant* otherwise. The Kendall rank correlation is defined between the n^{th} booking patterns in legs ij and pq as:

$$\rho_n(ij, pq) = \frac{t_c - t_d}{\sqrt{(t_0 - t_1)(t_0 - t_2)}} \quad (36)$$

where t_c is the number of concordant pairs, t_d is the number of discordant pairs, and t_0 , t_1 , and t_2 are defined as follows:

$$t_0 = \frac{T(T-1)}{2}, \quad (37)$$

$$t_1 = \sum_s u_s(u_s - 1)/2, \quad (38)$$

$$t_2 = \sum_t v_t(v_t - 1)/2, \quad (39)$$

where u_s is the number of tied values in the s^{th} group of ties for in booking patterns for leg ij , and v_t is analogous for leg pq . Then:

$$\rho(ij, pq) = \frac{1}{N} \sum_{n=1}^N \rho_n(ij, pq). \quad (40)$$

We compare the cases where the correlation measure is (i) applied directly to the booking patterns, and (ii) applied to the differenced booking patterns where the

within-booking pattern relationships e.g. trend have been removed. The normalised mutual information between the clustering produced by the correlation-based clustering under each of the different correlation measures, and the benchmark clustering is shown in Table 8.

Case	Correlation Measure	Fraction of Leg Demand Resulting from Cluster Itinerary Demand					
		50%	60%	70%	80%	90%	100%
Case 1	Booking patterns						
	Functional dynamical correlation	0.99	1.00	1.00	1.00	1.00	1.00
	Pearson correlation	1.00	1.00	1.00	1.00	1.00	1.00
	Kendall rank correlation	1.00	1.00	1.00	1.00	1.00	1.00
	Differenced booking patterns						
	Functional dynamical correlation	0.99	1.00	1.00	1.00	1.00	1.00
	Pearson correlation	0.98	1.00	1.00	1.00	1.00	1.00
	Kendall rank correlation	1.00	1.00	1.00	1.00	1.00	1.00
Case 2	Booking patterns						
	Functional dynamical correlation	0.98	0.99	1.00	1.00	1.00	1.00
	Pearson correlation	0.00	0.00	0.00	0.00	0.00	0.00
	Kendall rank correlation	0.00	0.00	0.00	0.00	0.00	0.00
	Differenced booking patterns						
	Functional dynamical correlation	0.98	0.99	1.00	1.00	1.00	1.00
	Pearson correlation	0.00	0.00	0.00	0.00	0.00	0.00
	Kendall rank correlation	0.00	0.00	0.00	0.00	0.00	0.00
Case 3	Booking patterns						
	Functional dynamical correlation	0.94	0.97	0.99	1.00	1.00	1.00
	Pearson correlation	0.00	0.00	0.00	0.00	0.00	0.00
	Kendall rank correlation	0.00	0.00	0.00	0.00	0.00	0.00
	Differenced booking patterns						
	Functional dynamical correlation	0.93	0.96	0.99	1.00	1.00	1.00
	Pearson correlation	0.00	0.00	0.00	0.00	0.00	0.00
	Kendall rank correlation	0.00	0.00	0.00	0.00	0.00	0.00

Table 8: Normalised mutual information under different correlation measures

For case 1, all three correlation measure seem to be performing equally well, with the normalised mutual information almost always indicating congruence. For cases 2 and 3, the Pearson and Kendall correlation results in extremely poor performance in terms of NMI, with the benchmark clustering never being achieved. Functional dynamical correlation, however, continues to perform well with an NMI close to 1.

In order to determine why the Pearson and Kendall rank correlations initially appear to perform well in the single cluster case, but fail in the two cluster case, we

also compare the value of the correlation coefficient with the known demand share in a simple two leg example. Consider the simple two leg network shown in Figure 25.

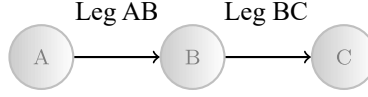


Figure 25: Network with two legs

The common traffic ratio of legs AB and BC is:

$$r(AB, BC) = \frac{D_{AC}}{D_{AB} + D_{BC} + D_{AC}}, \quad (41)$$

If $r(AB, BC) = 1$, then the number of bookings on leg AB and leg BC are identical, and the correlation between them is 1. Conversely, if $r(AB, BC) = 0$, then the bookings on leg AB and leg BC are independent with correlation 0. Table 9 shows the estimates of the correlation, compared to the true ratio, $r(AB, BC)$.

$r(AB, BC)$	0.0	0.1	0.2	0.3	0.4	0.5	0.6	0.7	0.8	0.9	1.0
Correlation between booking patterns											
Functional dynamical correlation	0.12	0.22	0.35	0.40	0.46	0.55	0.66	0.82	0.86	0.90	1.00
Pearson correlation	0.99	0.99	0.99	1.00	1.00	1.00	1.00	1.00	1.00	1.00	1.00
Kendall rank correlation	0.99	0.99	0.99	0.99	0.99	0.99	0.99	0.99	1.00	1.00	1.00
Correlation between differenced booking patterns											
Functional dynamical correlation	0.14	0.18	0.29	0.42	0.50	0.53	0.66	0.83	0.88	0.91	1.00
Pearson correlation	0.70	0.71	0.77	0.82	0.85	0.89	0.92	0.95	0.96	0.98	1.00
Kendall rank correlation	0.88	0.90	0.91	0.91	0.92	0.94	0.94	0.95	0.96	0.97	1.00

Table 9: Comparison of correlation measures

Functional dynamical correlation, applied directly to the data, performs best in all cases. In case 1, where the benchmark clustering is a single cluster, poor clustering performance can only result from under-estimating the demand share. Both Pearson and Kendall rank correlation over-estimate the correlation between booking patterns, even when the within-booking pattern effects have been removed. This explains the good performance of Pearson and Kendall rank correlation in case 1, despite extremely poor performance in cases 2 and 3.

D.2 Detecting outliers in multiple legs

D.2.1 Distribution of outliers across multiple legs

In the scenario where all itineraries are equally affected, a high proportion of outliers should be detected in more than one leg. Figure 26a illustrates the proportion of outliers detected in 1, 2, 3 or 4 legs: More than half were detected in multiple legs. Figure 26b shows the proportion of true positives (genuine outliers which were detected), by the number of legs in which they were detected. In contrast with Figure 26a, a much higher percentage of genuine outliers are detected in all four legs.

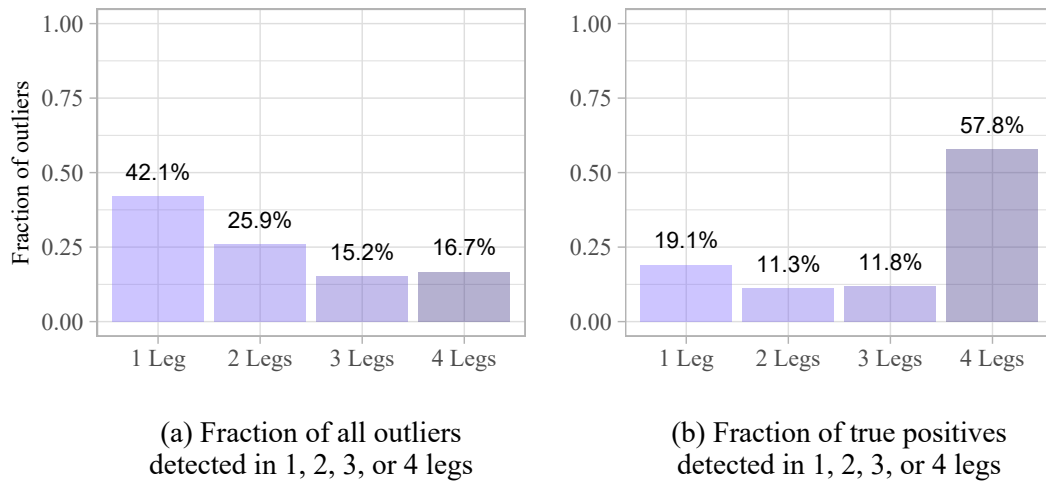


Figure 26: Fraction of outliers detected in 1, 2, 3, or 4 legs

Given the clustering is correct, we expect an approximately equal number of single leg outliers in each leg, as shown in Figure 27b. If one leg, say DE, had not belonged in this cluster, we would expect a higher proportion of single leg outliers to have been detected in leg DE. This could be utilised as a method for checking the clustering, after the outlier detection.

These results motivate aggregating threshold exceedances across legs in two ways: (i) since less than 100% of genuine outliers were detected in all legs, if outlier detection was carried out only on the leg level, outliers could be missed on some legs. (ii) Given that a much higher proportion of outliers detected in four legs were genuine outliers, by ranking booking patterns detected in all legs as more likely to be outliers, we focus analysts' attention to those more likely to be genuine outliers.

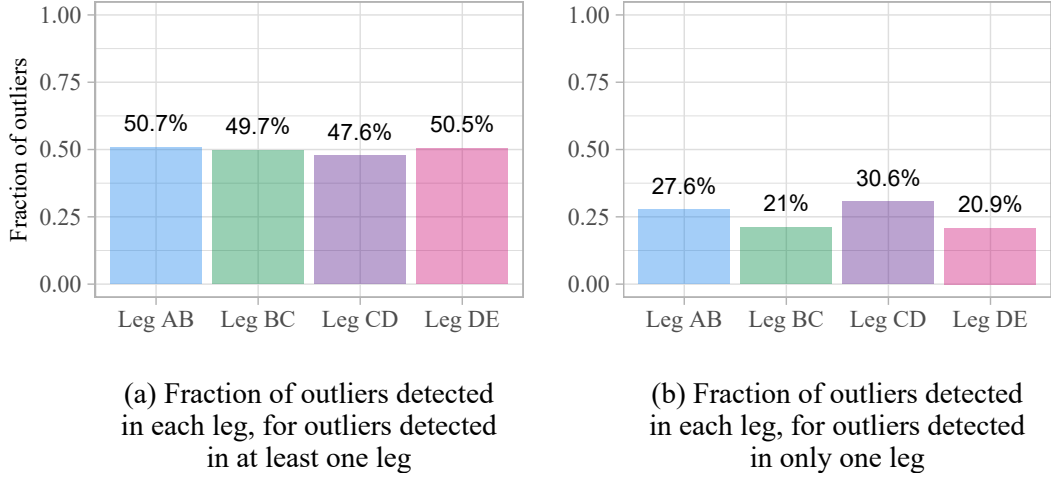


Figure 27: Fraction of outliers detected in each leg

D.2.2 False Discovery Rate

The *false discovery rate* (FDR) is defined as the proportion of booking patterns classified as outliers which were false positives:

$$FDR = \frac{FP}{TP + FP} \quad (42)$$

See Section 5.1 for definitions of true and false positives. Figure 28 shows the FDR for the case where outlier demand affects all itineraries, and the magnitude is randomly chosen from each of the distributions described in Section 4.3.

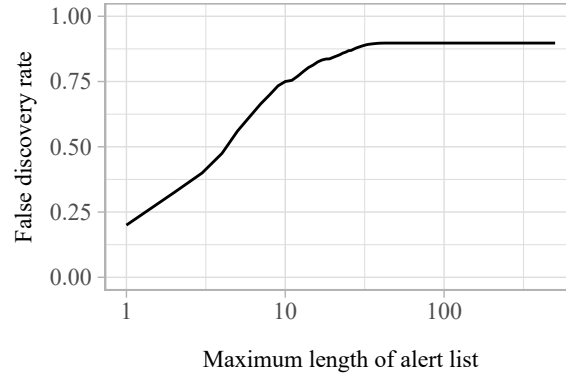


Figure 28: False discovery rate for nonhomogeneous demand-volume outliers

Figure 29 shows the FDR for each of the magnitudes of outliers considered in the simulation study. Given that smaller magnitude outliers are more similar to the regular demand, these result in higher false discovery rates.

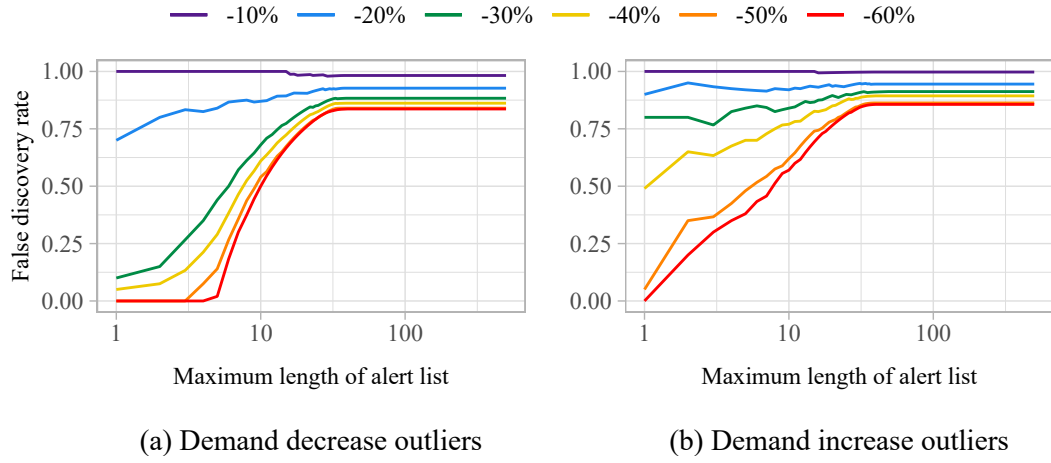


Figure 29: False discovery rate for homogeneous demand-volume outliers by magnitude

D.2.3 Outliers affecting a single itinerary

Figure 30 shows the true positive rate for the remaining itineraries in Figure 15 of Section 5.1.

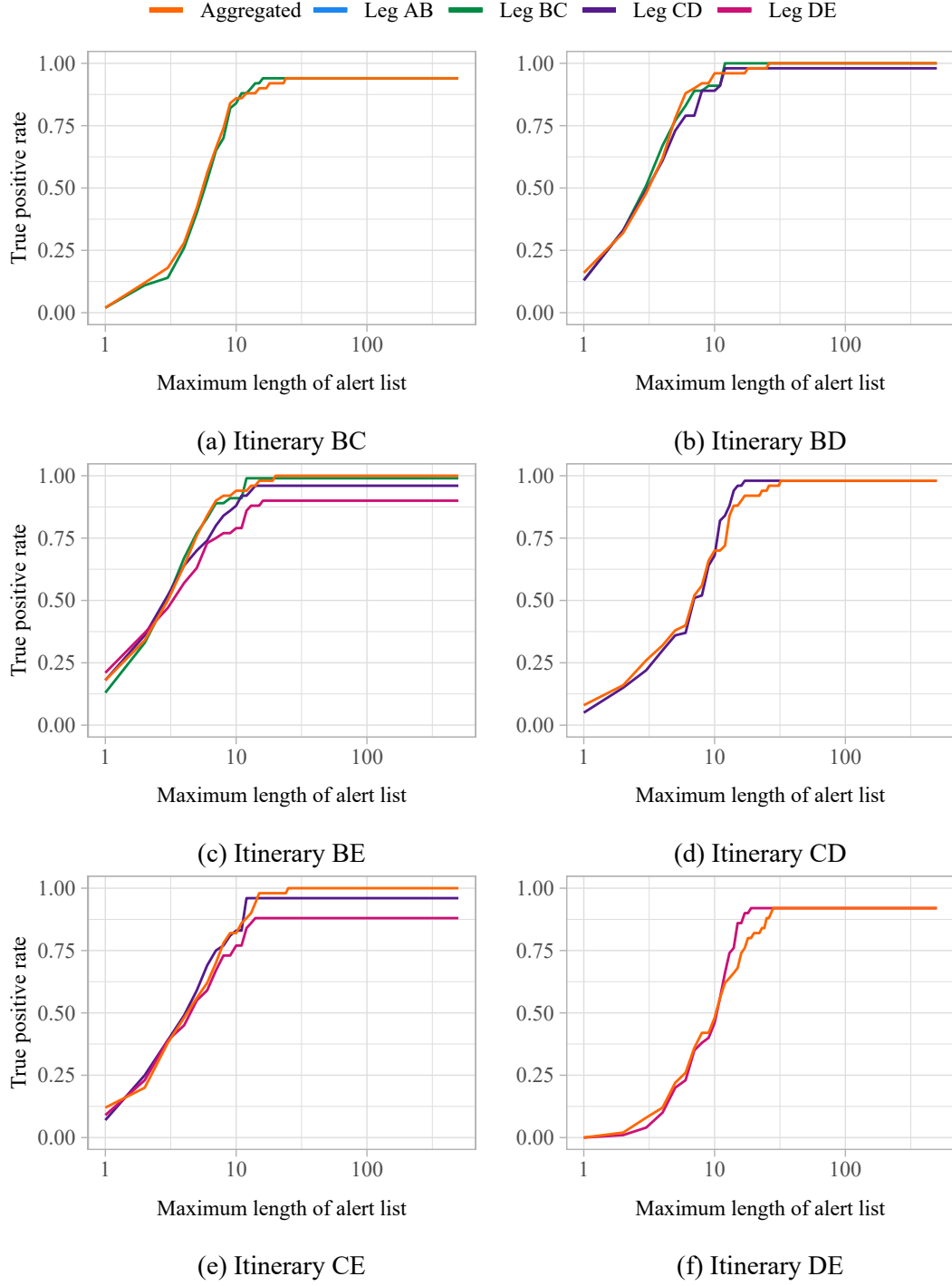


Figure 30: True positive rate for single itinerary outliers (cont.)

D.2.4 Outliers affecting a subset of itineraries

We consider a case where demand outliers affect only a subset of itineraries. Practical examples for this phenomenon could include trade fairs or conventions as well as regional crises. In such situations, demand towards (or from) a specific destination is most affected. Here, clustering offers additional benefits in guiding analysts towards those itineraries where they should adjust the forecast or controls.

We differentiate four scenarios based on the four-leg-network described in Section 4, where events affect demand for itineraries travelling to stations B, C, D, and E respectively. We expect analogous results when customers aim to travel home from events that happened at stations A, B, C, or D respectively, given the symmetry of the demand parameters chosen for the computational study.

For each of the four possible events considered, we investigate the case where this generates 50% increase in average leg demand. For simplicity, we assume these passengers are equally split between the itineraries which alight at the relevant station. Table 10 shows the resulting demand increases for each leg.

Event at Station	Itineraries Affected	Additional 120 Passengers in Itineraries			
		Resulting Demand Increase per Leg			
		Leg AB	Leg BC	Leg CD	Leg DE
B	A-B	+120 (+50%)	-	-	-
C	A-C, B-C	+60 (+25%)	+120 (+50%)	-	-
D	A-D, B-D, C-D	+40 (+16.6%)	+80 (+33.3%)	+120 (+50%)	-
E	A-E, B-E, C-E, D-E	+30 (12.5%)	+60 (+25%)	+90 (+37.5%)	+120 (+50%)

Table 10: Changes in leg demand resulting from an additional 120 passengers in itinerary demand

Figure 31a shows the true positive rate for each of the cases. Although the event at E generates outliers in more legs, it is not the case that it has the highest true positive rate. This shows that though the approach aggregates across legs, it does not ignore outliers only in a subset of those legs, provided they are sufficiently large. These effects may also be caused by interactions between the booking limits on different legs. For example, in the case of an event at C, large increases in demand in legs AB and BC may cause booking limits to be reached earlier for these legs, which also limits bookings in itineraries such as AD and AE. Hence, an increase in demand for some legs may caused a decrease in bookings for different legs. By jointly considering multiple legs for outlier detection, we are able to detect the knock-on effects of outliers even when the change in demand only affects a subset of legs. The change in precision can be interpreted similarly, in Figure 31b.

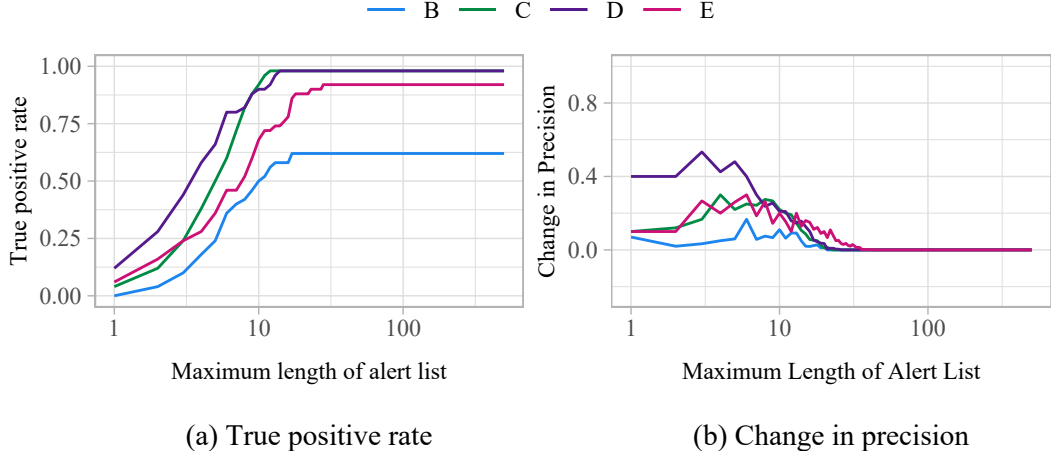


Figure 31: Performance for demand-volume outliers in a subset of itineraries caused by an absolute increase in demand

Had we considered outlier detection on a leg-by-leg basis, the outliers were more likely to be missed in some of the legs. By combining information across legs, we are better able to determine which itineraries are affecting the volume of demand.

D.2.5 Using outlier severity threshold to limit alert list length

The results in this paper focus on limiting the length of the ranked alert list simply by the number of alerts it contains as this is most relevant to analysts. However, an alternative approach limits the length of the list by the outlier severity assigned to each departure. For example, classifying a train as an outlier only if its outlier severity is above 80%.

Detection results when outliers affect all itineraries

Figure 32 shows the true positive rate as the outlier severity decreases from 100% to 0%. Results are similar to those shown in Figure 11a. Figure 33 shows the true positive rate as the outlier severity decreases from 100% to 0%, for each magnitude of outlier considered. Results are similar to those shown in Figure 13.

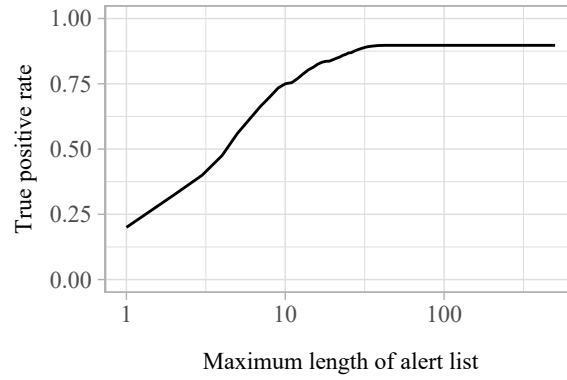


Figure 32: True positive rate for nonhomogeneous demand-volume outliers as minimum outlier severity varies

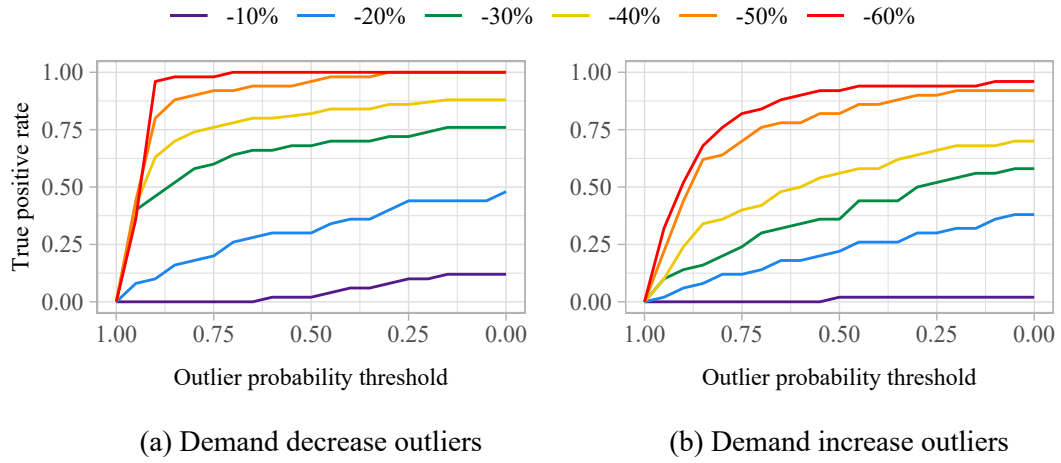


Figure 33: True positive rate for homogeneous demand-volume outliers by magnitude

Detection results when outliers affect a single itinerary

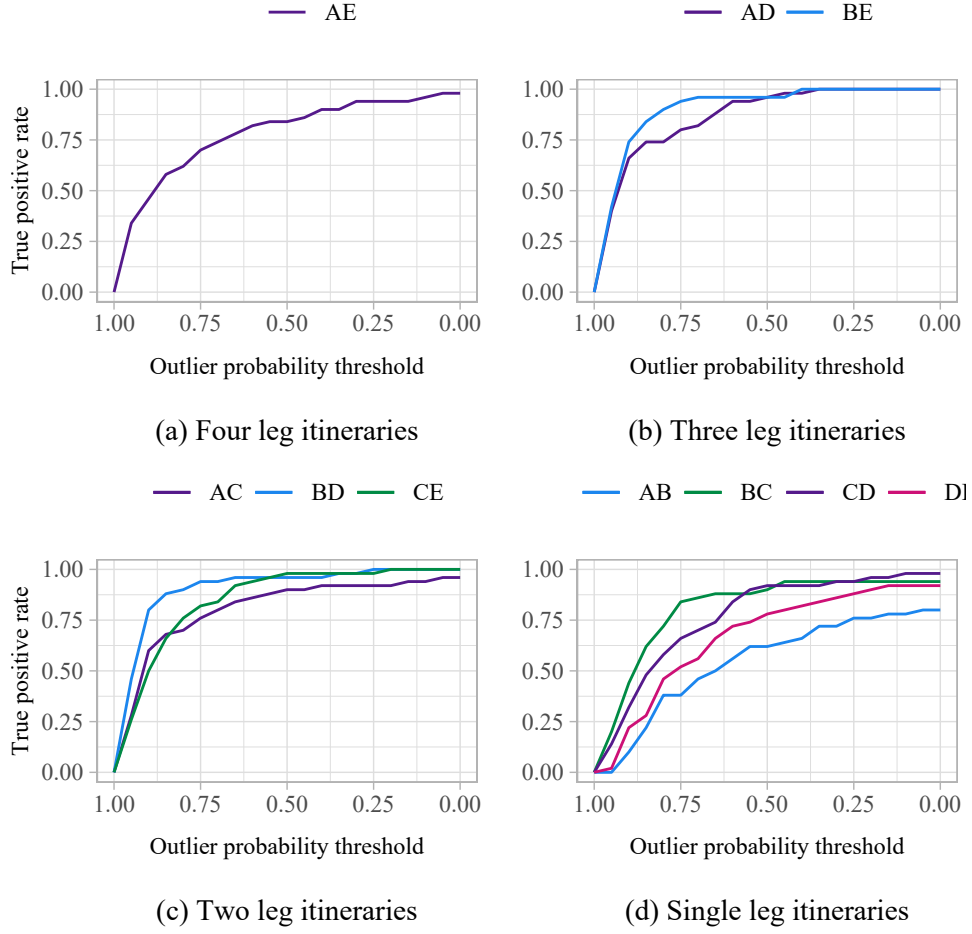


Figure 34: True positive rate for single itinerary demand-volume outliers as minimum outlier severity varies

D.3 Revenue benefits from forecast adjustments for outlier demand

Figure 35 shows the true positive rate for the remaining itineraries in Figure 16 of Section 5.2.

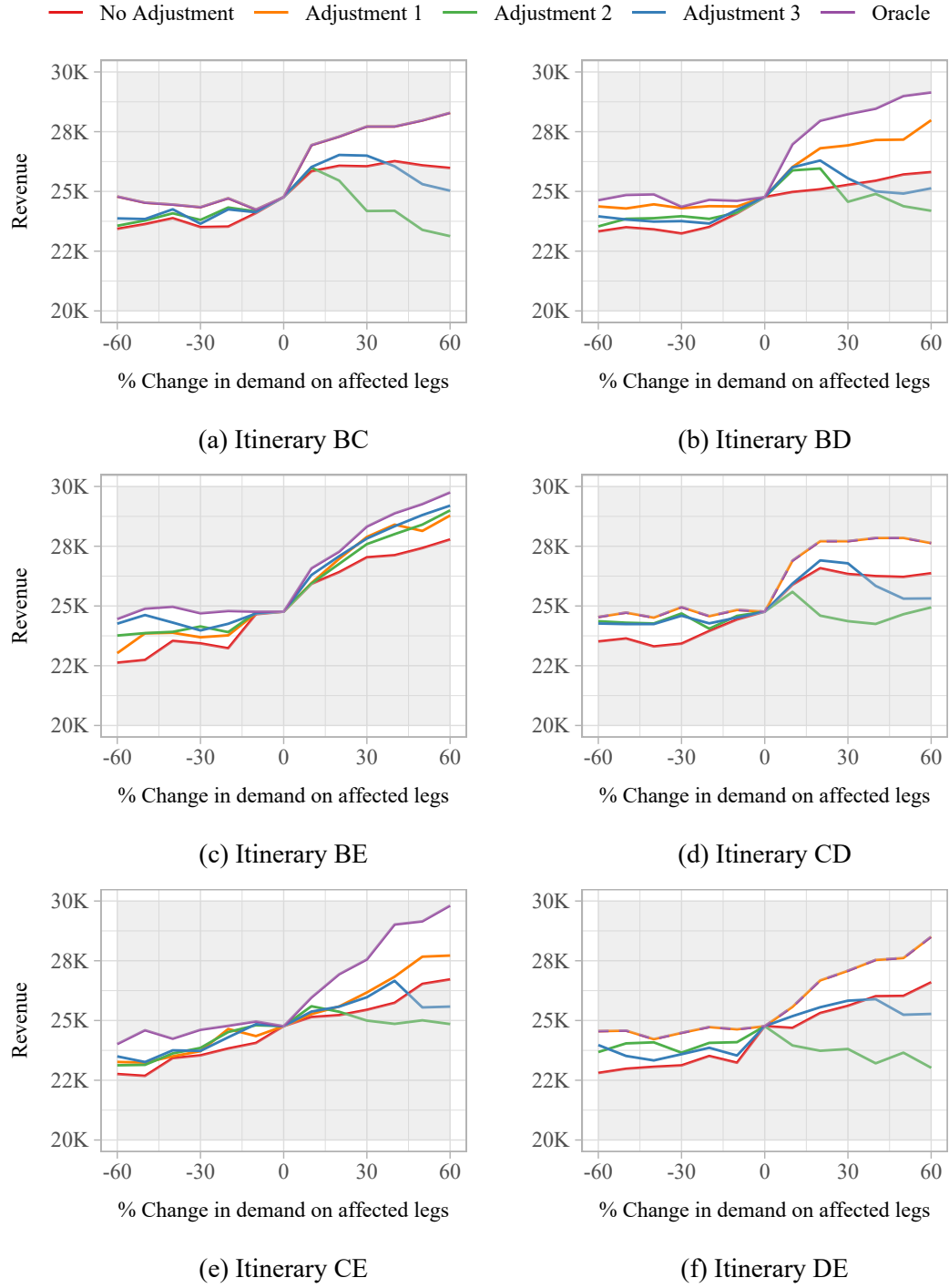


Figure 35: Revenue generated under different itinerary-level forecast adjustments (cont.)

The analysis in Section 4.4 constitutes a best-case scenario in which we assume that, if outlier demand affects a particular leg, the outlier is detected in that leg.

However, as we show in Section 5.1, even when demand outliers affect multiple legs, the outlier is not always detected in every leg due to noise. Therefore, we additionally compare different adjustments based on the output of the outlier detection, for an outlier in itinerary AE.

- **Adjustment A:** Adjust only the forecasts of the affected single-leg itineraries for those legs in which the outlier is detected.
- **Adjustment B:** Adjust the forecasts of the affected single-leg itineraries for those legs in which the outlier is detected, **and** the cluster spanning itinerary (AE).

We compare these both to making no adjustment, and to the oracle adjustment. This is still a best-case scenario to some extent, given that we assume the correct magnitude of adjustment is made.

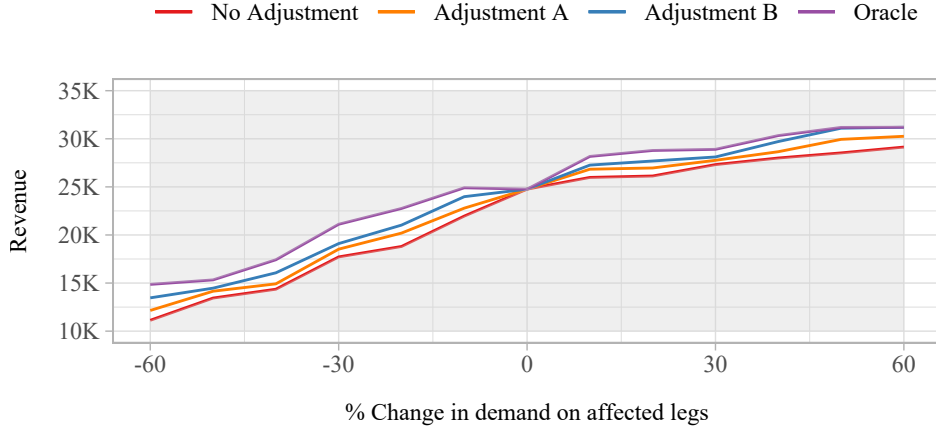


Figure 36: Revenue generated under different forecast adjustments resulting from the outlier detection for outlier demand in itinerary AE

Figure 36 shows the revenue under adjustments A and B (as described in Section 4.4) depending on the output of the outlier detection procedure. Combining adjustments on the leg-level with those on the cluster level provides superior results in contrast to leg level adjustments alone. Though making adjustments to only the single-leg itineraries may be risk averse in the rare cases where an outlier affects only a small subset of the legs within a cluster, it may be detrimental to revenue when outliers affect multiple legs.